tapraid4/zh2-aflu/zh2-aflu/zh200308/zh25047d08z | xppws | S=1 | 1/29/08 | 2:16 | MS: F-00201-2007 | lni: 03/dmp/dlh

Table 2. *Defects in urinary concentration in TazlacZ/lacZ mice*

	Taz+/+	*TazlacZ/lacZ*
n	6	6
Age, wk	20–26	20–26
Body wt, g	36.8±2.1	29.4±3.1*
Water intake, ml/day	6.7±1.4	17.5±2.4*
Urine volume, ml/day	3.56±1.39	10.76±3.02*
Osmolality, mosmol/kgH_2O	2,765±646	855±131*
Urine nitrogen, mg·day^{-1}·g body wt^{-1}	4.11±0.84	3.29±1.36
Creatinine, g·day^{-1}·g body wt^{-1}	32.3±7.0	34.5±13.3
Albumin, g·day^{-1}·g body wt^{-1}	1.91±1.02	29.60±42.49
Na^+, meq·day^{-1}·g body wt^{-1}	0.011±0.004	0.011±0.002
K^+, meq·day^{-1}·g body wt^{-1}	0.034±0.007	0.035±0.009
Cl^-, meq·day^{-1}·g body wt^{-1}	0.017±0.003	0.022±0.006†

Values are means ± SD. *$P < 0.01$ and †$P < 0.05$.

greater in $Taz^{lacZ/lacZ}$ mice (149.6 ± 11.5 μm, $n = 4$) than in wild-type mice (51.6 ± 2.1 μm, $n = 4$) (Fig. 3*C*). There were no findings indicative of increased inflammation or fibrosis in $Taz^{lacZ/lacZ}$ lungs. The phenotype of $Taz^{lacZ/lacZ}$ lungs is highly reminiscent of human pulmonary emphysema.

The changes in the kidney and lung were observed in all the homozygous mice derived from two independent recombinant ES clones, although the severity of symptoms varied among individuals. In contrast, no wild-type and $Taz^{+/lacZ}$ mice displayed abnormalities (Figs. 2, *A* and *B*, and 3*A*).

Urinary concentration defects in $Taz^{lacZ/lacz}$ mice. In addition to multiple cysts and dilated calyces, $Taz^{lacZ/lacZ}$ mice showed signs of polyuria. Indeed, the urinary bladder in $Taz^{lacZ/lacZ}$ mice was typically distended with a large volume of urine (data not shown). Measurement of the 48-h urine frequency and volume revealed that urine volume per void and total volume per day were much higher in $Taz^{lacZ/lacZ}$ mice than in $Taz^{+/lacZ}$ mice (Fig. 4). Measurements of urinary parameters showed polyuria and concentrating defects in $Taz^{lacZ/lacZ}$ mice, as indicated by lower urinary osmolality (Table 2). Overall electrolyte excretion was not enhanced, although excretion of chloride was slightly increased (Table 2), indicating that electrolyte reabsorption remained grossly preserved. Urinary albumin excretion in $Taz^{lacZ/lacZ}$ mice appeared to be increased, although the difference was not statistically significant (Table 2). The polyuria and concentrating defects in $Taz^{lacZ/lacZ}$ mice were not improved by vasopressin administration (data not shown), suggesting that the abnormalities were likely to be nephrogenic rather than due to vasopressin deficiency. Overall, $Taz^{lacZ/lacZ}$ kidneys were characterized by the concomitant occurrence of features that are typical of human PKD, including multicystic formation and urinary concentrating defects, and atypical features such as calyceal dilatation and hydronephrosis.

Cysts primarily originated from glomeruli and proximal tubules in $Taz^{lacZ/lacz}$ embryos. To determine the time point at which cysts first arose in the kidneys of $Taz^{lacZ/lacZ}$ embryos, we performed histological analysis on kidneys at different embryonic stages. At *embryonic day 13.5*, the branching of ureteric buds and the initial formation of renal vesicles and comma- and S-shaped bodies appeared to be normal in both $Taz^{lacZ/lacZ}$ and wild-type kidneys (Fig. 5, *A* and *B*). At *embryonic day 15.5*, morphological abnormalities were first detected as dilatation of the Bowman's capsules and adjacent tubules in $Taz^{lacZ/lacZ}$ embryos (Fig. 5, *C* and *D*).

At *embryonic day 18.5*, $Taz^{lacZ/lacZ}$ kidneys exhibited tubules with varying degrees of dilatation and multiple cysts in inner cortical and medullary regions (Fig. 5, *E* and *F*). Cyst-lining epithelial cells appeared heterogeneous in morphology; some were flattened and others were rather cuboidal (Fig. 5, *G* and *H*). Glomerular tufts were detected in a small subset of cysts at this stage (Fig. 5, *G* and *H*). The renal pelvis was dilated, and the medulla was atrophic with disturbed formation of the papilla (Fig. 5, *E* and *F*). In contrast, the nephrogenic zone was well-developed in the outer cortex just beneath the capsule and contained many developing nephrons in $TAZ^{lacZ/lacZ}$ and wild-type kidneys (Fig. 5, *E–H*).

We examined the origins of the cysts using segment-specific markers. LTA, a lectin specific for the proximal tubule, stained the majority of epithelial cells lining dilated tubules and cysts in *embryonic day 18.5* $Taz^{lacZ/lacZ}$ embryos (Fig. 6, *A–D*). In contrast, no cysts were stained with DBA, a lectin specific for the collecting duct, at the same stage (Fig. 6, *E–H*). These results suggested that the cystic changes in $Taz^{lacZ/lacZ}$ kidneys primarily originated from glomeruli and proximal tubules during the maturation of induced nephrons.

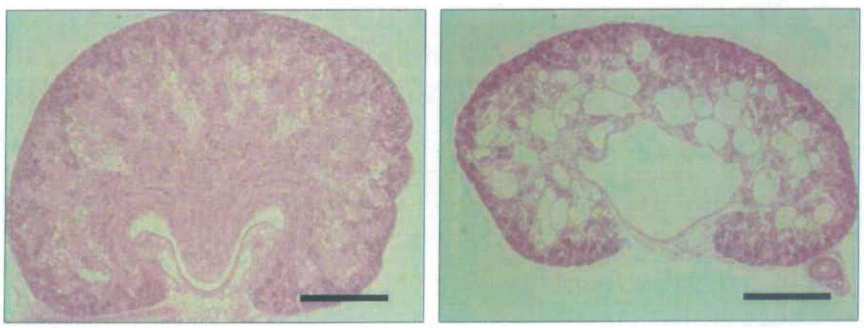

COLOR

Fig. 5. Histological examination of developing kidneys in control (*A*, *C*, *E*, and *G*) and $Taz^{lacZ/lacZ}$ (*B*, *D*, *F*, and *H*) embryos. *A* and *B*: at *embryonic day 13.5*, branching of ureteric buds and formation of renal vesicles and comma- and S-shaped bodies are observed in $Taz^{lacZ/lacZ}$ (*B*) as well as wild-type and $Taz^{+/lacZ}$ (*A*) kidneys. *C* and *D*: at *embryonic day 15.5*, dilatation of Bowman's capsules (arrows) and adjacent tubules (arrowheads) are detected in $Taz^{lacZ/lacZ}$ kidneys (*D*) but not in wild-type kidneys (*C*). *E–H*: at *embryonic day 18.5*, the atrophic medulla contains multiple cysts of various sizes in $Taz^{lacZ/lacZ}$ kidneys (*F* and *H*). The pelvis is dilated and the papilla is not well formed (*F*). These changes are not observed in wild-type kidneys (*E* and *G*). The nephrogenic zone is present in the outer cortex just beneath the capsule in $Taz^{lacZ/lacZ}$ (*H*) and wild-type (*G*) kidneys. Scale bars indicate 100 μm (*A–D*, *G*, and *H*) and 500 μm (*E* and *F*).

tapraid4/zh2-aflu/zh2-aflu/zh200308/zh25047d08z | xppws | S=1 | 1/29/08 | 2:16 | MS: F-00201-2007 | Ini: 03/dmp/dlh

COLOR

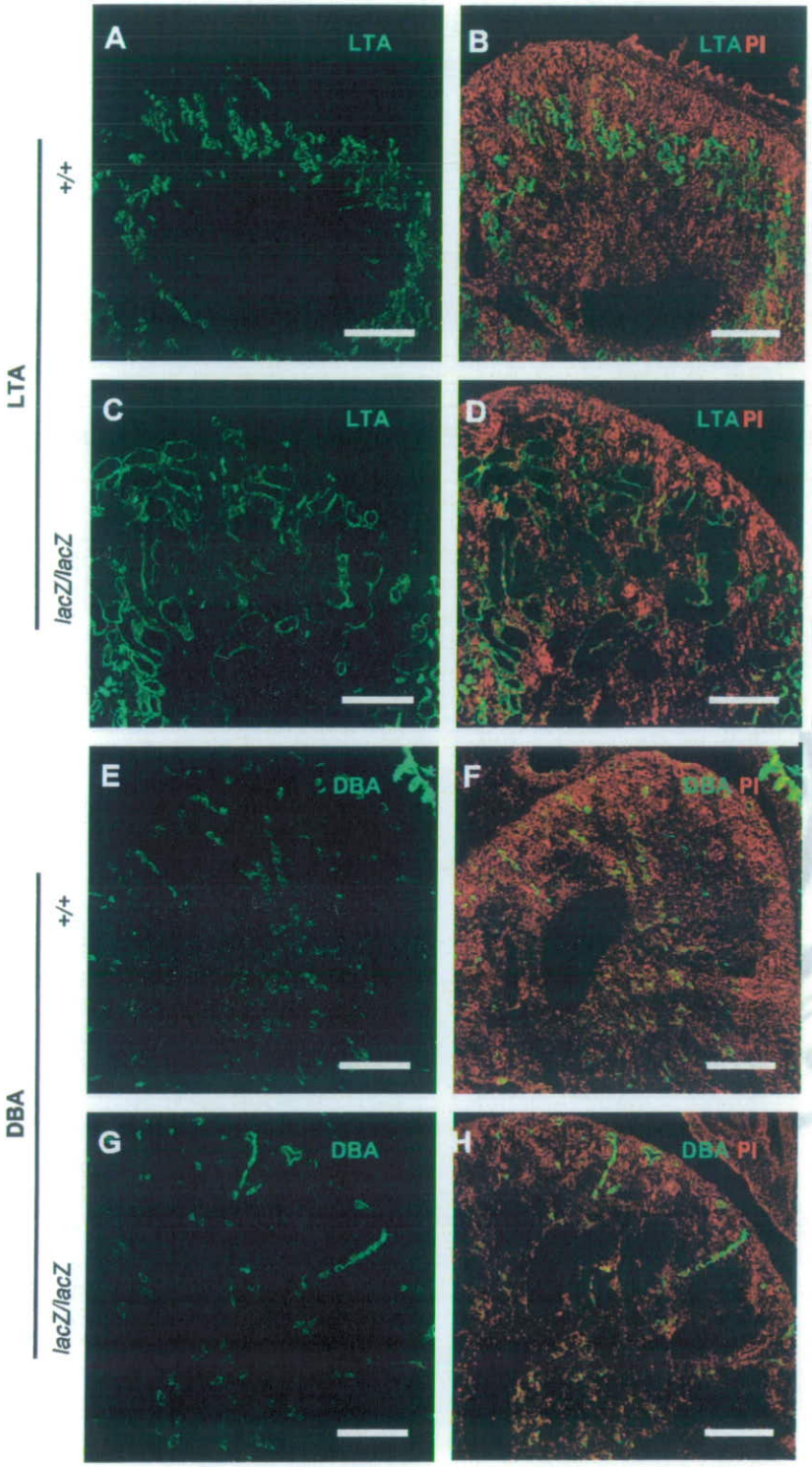

Fig. 6. Proximal tubular dilatation leading to cyst formation in $Taz^{lacZ/lacZ}$ embryos. Sections were stained with *Lotus tetragonolobus* agglutinin (LTA; *A–D*) or *Dolichos biflorus* agglutinin (DBA; *E–H*) in wild-type (*A*, *B*, *E*, and *F*) and $Taz^{lacZ/lacZ}$ (*C*, *D*, *G*, and *H*) kidneys at *embryonic day 18.5*. *B*, *D*, *F*, and *H* show costaining with propidium iodide and lectins. Epithelial cells lining dilated tubules and cysts stain positive with LTA but not with DBA in $Taz^{lacZ/lacZ}$ kidneys. Scale bars indicate 250 μm.

Expression of Taz in developing kidneys. To correlate the renal phenotype of $Taz^{lacZ/lacZ}$ mice with *Taz* expression, we first performed in situ hybridization on wild-type embryonic kidneys. At *embryonic day 14.5*, *Taz* transcripts were diffusely expressed in both mesenchymal and epithelial cells in the developing metanephros (Fig. 7, *A* and *B*). *Taz* was also present in the ureteric bud (Fig. 7, *A* and *B*). At *embryonic day 16.5*, *Taz* was expressed in mesenchymal and epithelial cells in the nephrogenic zone and collecting ducts (Fig. 7, *C* and *D*). F7

tapraid4/zh2-aflu/zh2-aflu/zh200308/zh25047d08z | xppws | S=1 | 1/29/08 | 2:16 | MS: F-00201-2007 | Ini: 03/dmp/dlh

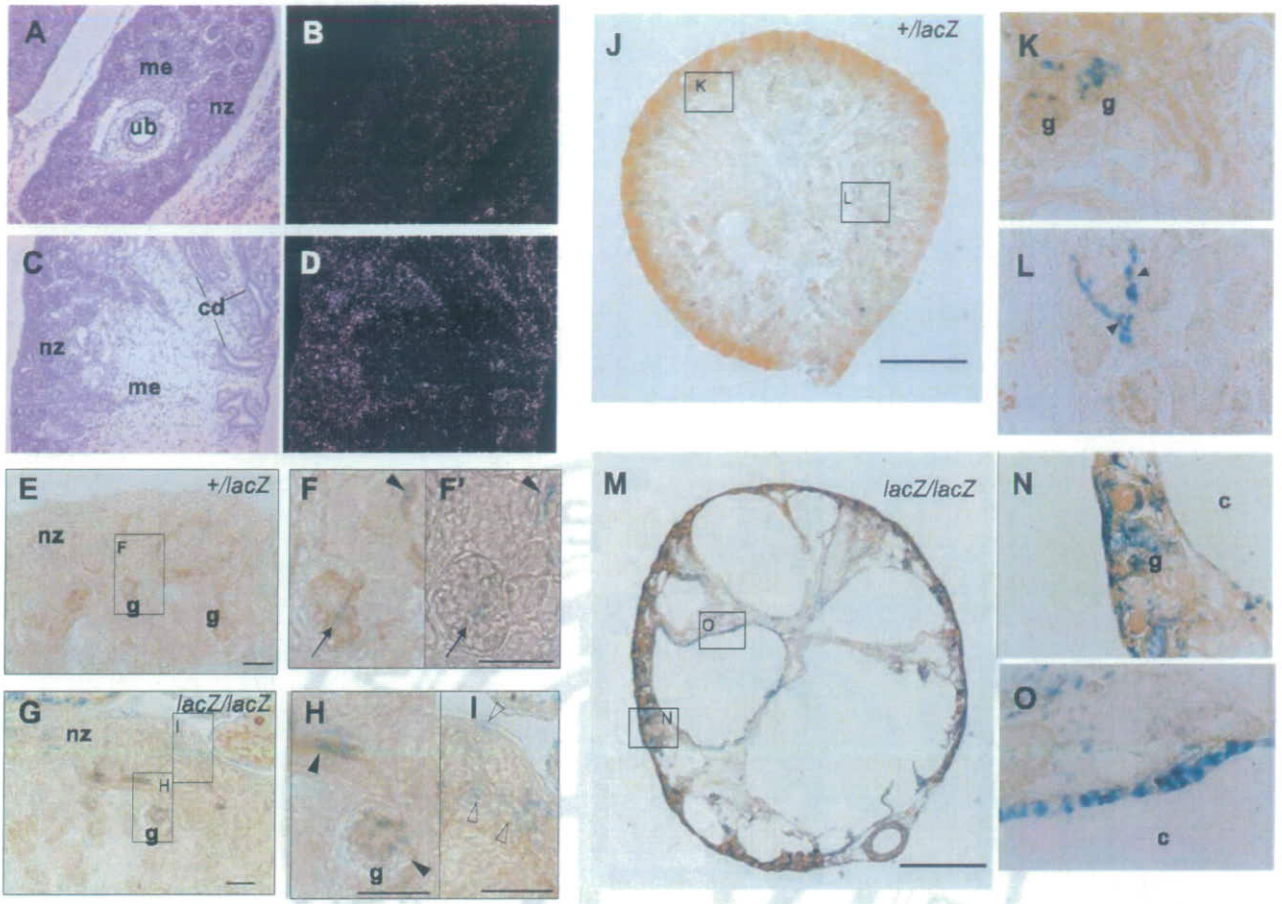

Fig. 7. *Taz* expression during metanephric development. *A–D*: in situ hybridization of mouse embryonic kidneys with probes for *Taz*. Brightfield (*A* and *C*) and darkfield (*B* and *D*) images of *embryonic day 14.5* (*A* and *B*) and *embryonic day 16.5* (*C–F*) kidneys are shown. *A* and *B*: at *embryonic day 14.5*, *Taz* transcripts are diffusely detected in metanephric mesenchymal and epithelial cells and the ureteric bud. *C* and *D*: at *embryonic day 16.5*, *Taz* is expressed in mesenchymal and epithelial cells in the nephrogenic zone. *Taz* is also expressed in the collecting ducts. *E–O*: β-galactosidase activity in $Taz^{+/lacZ}$ (*E*, *F*, and *J–L*) and $Taz^{lacZ/lacZ}$ (*G–I* and *M–O*) kidneys at *embryonic day 16.5* (*E–I*) and *day 0* postpartum (P0; *J–O*). *E*, *F*, and *F'*, in *embryonic day 16.5* $Taz^{+/lacZ}$ kidneys, X-gal staining (blue) is observed in glomeruli (arrows) and CD31-stained (brown) capillary endothelial cells (arrowheads). X-gal staining with (*F*) and without (*F'*) CD31 staining is shown. *G–I*: in *embryonic day 16.5* $Taz^{lacZ/lacZ}$ kidneys, X-gal staining is observed in stromal(-like) cells (open arrowheads in *I*) as well as in glomeruli and capillary endothelial cells (filled arrowheads in *H*). *J–L*: in P0 $Taz^{+/lacZ}$ kidneys, scattered X-gal staining is observed in glomeruli (*K*) and capillary endothelial cells (*L*). *M–O*: in P0 $Taz^{lacZ/lacZ}$ kidneys, X-gal staining is observed in outer cortical stromal cells, glomeruli, and capillaries (*N*). Some cysts are lined by X-gal-positive cells (*O*). Sections of P0 kidney were counterstained with Orange G. c, cyst; cd, collecting duct; g, glomerulus; me, mesenchyme; nz, nephrogenic zone; ub, ureteric bud. Scale bars indicate 50 μm (*E* and *I*) and 500 μm (*J* and *M*).

In contrast to in situ hybridization, β-galactosidase activity was observed only in limited cell populations. At *embryonic day 16.5* and *day 0* postpartum, $Taz^{+/lacZ}$ kidneys exhibited sporadic *lacZ* expression in glomeruli and capillary endothelial cells that were positive for CD31 (Fig. 7, *E*, *F*, and *J–L*), indicating that *lacZ* expression may only reflect a part of the authentic *Taz* expression, possibly due to disruption of critical genomic sequences. In $Taz^{lacZ/lacZ}$ homozygous kidneys, β-galactosidase activity was detected in stromal(-like) cells, especially in the outer cortical region as well as in glomeruli and capillary endothelial cells (Fig. 7, *G–I*, *M*, and *N*). In addition, some cysts are lined by *lacZ*-positive cells in *day 0* postpartum $Taz^{lacZ/lacZ}$ kidneys (Fig. 7*O*).

Expression of cystic disease transcripts and proteins in $Taz^{lacZ/lacz}$ *kidneys.* To find clues to the mechanism underlying the renal phenotype of $Taz^{lacZ/lacZ}$ mice, we analyzed the expression of genes involved in human PKD. No alterations in the levels of *Pkd1* and *Pkd2* mRNA and their products, polycystin-1 and polycystin-2, were observed at *embryonic day 15.5* and *18.5* by real-time RT-PCR (Fig. 8, *A* and *B*) and Western blotting (Fig. 8*D*). Also, the expression of *Pkhd1*, a gene linked to ARPKD, was not different between wild-type and $Taz^{lacZ/lacZ}$ kidneys (Fig. 8*C*). These results indicated that renal cyst formation induced by *Taz*-null mutation was not due to changes in the expression of *Pkd1*, *Pkd2*, and *Pkhd1* at the perinatal stage. F8

Expression of genes involved in water metabolism in $Taz^{lacZ/lacz}$ *kidneys.* The absence of changes in the expression of cystic disease genes and concomitant diabetes insipidus-like state led us to speculate that unique pathogenetic mechanisms might underlie the renal phenotypes in $Taz^{lacZ/lacZ}$ kidneys. To explore the basis for disturbed water metabolism, we investigated the expression of genes and proteins that are involved in renal water transport. Although the urinary concentration defects in $Taz^{lacZ/lacZ}$ mice were resistant to exogenous vasopressin, real-time RT-PCR analysis showed that the expression of the

tapraid4/zh2-aflu/zh2-aflu/zh200308/zh25047d08z | xppws | S=1 | 1/29/08 | 2:16 | MS: F-00201-2007 | lni: 03/dmp/dlh

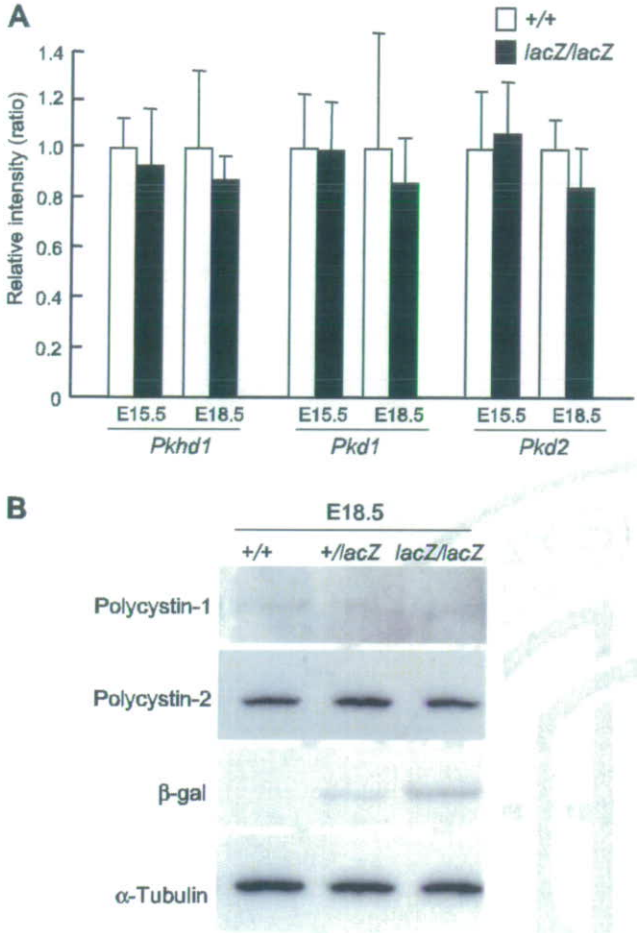

Fig. 8. Real-time RT-PCR analysis and Western blotting of cystic disease genes and proteins. *A*: real-time RT-PCR. Total RNA samples were prepared from *embryonic day 15.5* and *18.5* wild-type (*+/+*) and homozygous (*lacZ/lacZ*) kidneys. The abundance of transcripts for *Pkd1*, *Pkd2*, and *Pkhd1* was measured relative to the internal control *Gapdh*. Error bars indicate SDs of the mean (n = 5). For all threes genes at both stages, the expression in homozygous mutant kidneys is not statistically different from wild-type kidney ($P > 0.05$). *B*: Western blotting for polycystin-1 and polycystin-2. Protein levels of polycystin-1 and -2 are not different among wild-type, $Taz^{+/lacZ}$, and $Taz^{lacZ/lacZ}$ kidneys at *embryonic day 18.5*. Blotting for β-galactosidase shows intensities corresponding to the copy number of the *lacZ* gene. Blotting for α-tubulin serves as an internal control.

arginine vasopressin receptor 2 gene (*Avpr2*) was largely unaffected in $Taz^{lacZ/lacZ}$ kidneys (Fig. 9*A*). The expression of aquaporin (*Aqp-1*, *-2*, and *-3*) water channels that are involved in renal water reabsorption (28) was not different among wild-type, heterozygous, and homozygous mutant kidneys (Fig. 9*B*). Immunostaining demonstrated that aquaporin-3 was localized in the basolateral membrane of epithelial cells in both $Taz^{lacZ/lacZ}$ and control $Taz^{+/lacZ}$ kidneys (Fig. 9, *C* and *D*), indicating that the polarity of aquaporin-3 localization in $Taz^{lacZ/lacZ}$ epithelial cells was intact. In $Taz^{lacZ/lacZ}$ kidneys, aquaporin-3 was expressed in many noncystic tubules and a few cysts (Fig. 9*D*), indicating an origin from the renal collecting ducts. Aquaporin-2 was also expressed similarly in collecting ducts in heterozygous and homozygous kidneys at *embryonic day 18.5* (Fig. 9, *E* and *F*). These results indicated that the renal phenotype of $Taz^{lacZ/lacZ}$ mice was not caused by changes in the expression of *Avpr2* or aquaporins.

DISCUSSION

In the present study, we demonstrate that a null mutation of *Taz* results in the formation of bilateral multicystic kidneys and diffuse emphysematous changes in the lung. Renal cysts mainly originate from the glomeruli and proximal tubules around *embryonic day 15.5*, as revealed by histological features and lectin marker staining. Later, the renal changes are accompanied by pelvic dilatation and atrophy of the medulla, indicating hydronephrosis. After birth, only one-fifth of TAZ-deficient homozygotes grow to adulthood. The early mortality may be due to water and electrolyte imbalance and/or respiratory insufficiency. Surviving mutants demonstrate progressive renal changes with massive polyuria. The renal phenotype of TAZ-deficient mice is reminiscent of human renal cystic diseases, as represented by PKD, but is distinct in that it manifests as severe hydronephrosis and urinary concentration defects.

Comparison of the renal phenotype of TAZ-deficient mice to human cystic kidney diseases. In human ADPKD, the epithelial-lined cysts originate from any segment of the nephron and collecting ducts, and in ARPKD the cysts mainly originate from the collecting ducts (3, 10). In contrast, the cysts in TAZ-deficient kidneys mainly originate from the glomeruli and proximal tubules. However, patients with early onset ADPKD may develop glomerular cysts, suggesting that cyst formation in the proximal nephrons may be an early manifestation of ADPKD (11. 15). Consistently, *Pkd1*-null mice start to exhibit cyst formation at *embryonic day 15.5* in the proximal tubule (20). Other animal models of PKD, such as the *cpk/cpk* mice and the Han:SPRD *cy/+* rats, have also shown cysts originating predominantly from the proximal tubule (39). Studies of human fetuses with ARPKD have shown cysts originating from proximal tubules. Thus the renal phonotype of TAZ-deficient mice may recapitulate the early phase of human PKD.

However, no apparent differences in the expression of PKD genes, *Pkd1*, *Pkd2*, and *Pkhd1*, are detected in the kidneys of wild-type and TAZ-deficient embryos before birth. This finding indicates that cyst formation in TAZ-deficient kidneys is not due to changes in the expression of these cystic disease genes. Polycystin-1 and -2, proteins encoded by ADPKD genes *PKD1* and *PKD2*, respectively, are membrane glycoproteins that can associate with each other to form a complex in the primary cilium of renal epithelial cells (2, 10, 19). The polycystin complex is implicated in cell cycle regulation, intracellular calcium regulation, and maintenance of cellular polarity (2, 10, 19). Polyductin/fibrocystin, the protein encoded by *PKHD1*, is also a large transmembrane protein. Considering the possible interaction of TAZ with membrane-associated PDZ domain-containing proteins, it may still be possible that TAZ and the cystic disease proteins share a common pathway involved in normal epithelial function and structural integrity. However, taken together with the pathological differences from human PKD, distinct mechanisms may be involved in the renal phenotype of TAZ-deficient mice.

Recently, Hossain et al. (16) also reported the development of cystic kidney disease in TAZ/Wwtr1-deficient mice. Their study suggested that the loss of renal cilia integrity

tapraid4/zh2-aflu/zh2-aflu/zh200308/zh25047d08z | xppws | S=1 | 1/29/08 | 2:16 | MS: F-00201-2007 | Ini: 03/dmp/dlh

COLOR

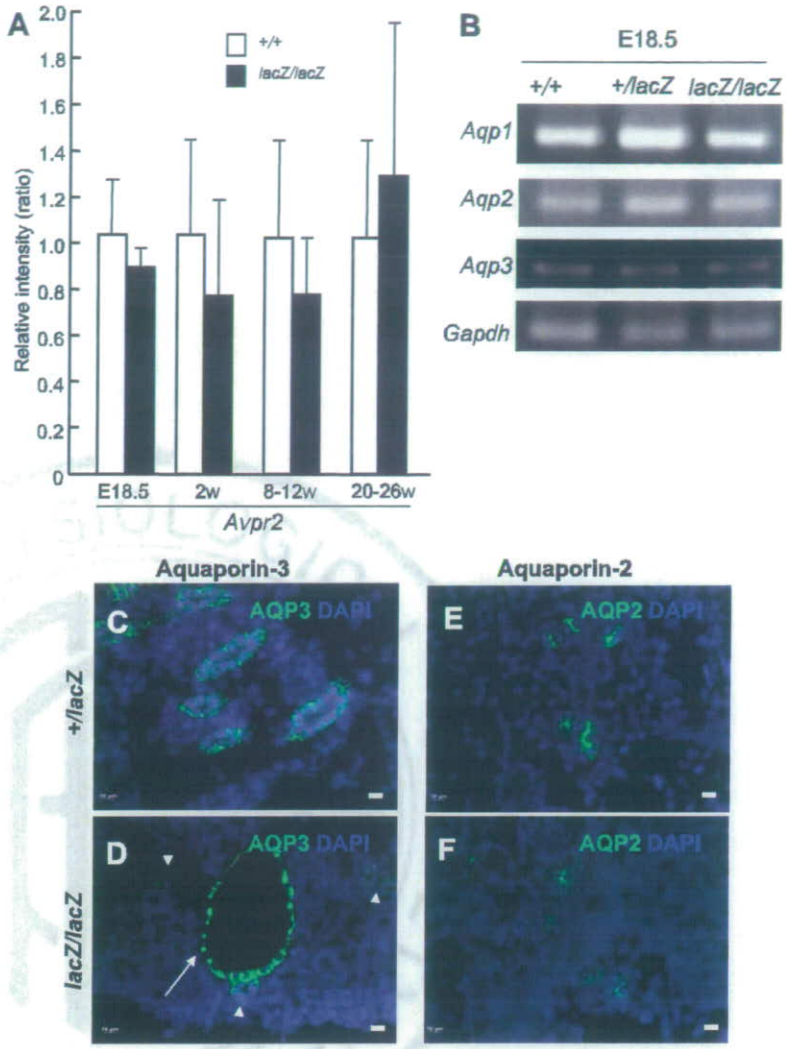

Fig. 9. Expression of genes involved in water transport. *A*: real-time RT-PCR. Total RNA samples were prepared from *embryonic day 18.5* and 2-wk-old wild-type (+/+) and homozygous (*lacZ/lacZ*) kidneys. The abundance of transcripts for *Avpr2* was measured relative to the internal control *Gapdh*. Error bars indicate SDs of the mean; $n = 5$ (+/+) and 5 (*lacZ/lacZ*) at *embryonic day 18.5*; $n = 4$ (+/+) and 3 (*lacZ/lacZ*) at 2 wk; $n = 8$ (+/+) and 6 (*lacZ/lacZ*) at 8–12 wk; $n = 4$ (+/+) and 4 (*lacZ/lacZ*) at 20–26 wk. No statistically significant difference is detected in the expression of *Avpr2* between +/+ and *lacZ/lacZ* kidneys ($P > 0.05$). *B*: RT-PCR analysis of *Aquaporin-1*, *-2*, and *-3* expression. Total RNA samples were prepared from *embryonic day 18.5* wild-type (+/+), heterozygous (+/*lacZ*), and homozygous (*lacZ/lacZ*) kidneys. The levels of *Aquaporin-1*, *-2*, and *-3* transcripts are not different among wild-type, heterozygous, and homozygous kidneys. RT-PCR for *Gapdh* served as an internal control. *C–F*: immunofluorescence staining of aquaporins. Sections were stained for aquaporin-3 (*C* and *D*) or aquaporin-2 (*E* and *F*) in $Taz^{+/lacZ}$ (*C* and *E*) and $Taz^{lacZ/lacZ}$ (*D* and *F*) kidneys at *embryonic day 18.5*. All sections were costained with 4′,6-diamidine-2-phenylindole. Aquaporin-3 is localized in the basolateral membrane of epithelial cells in some cysts (arrow) as well as in noncystic tubules (arrowheads) in $Taz^{lacZ/lacZ}$ kidneys. Aquaporin-2 is also expressed similarly in collecting ducts in heterozygous and homozygous kidneys. Scale bars indicate 10 μm.

and downregulation of several genes, including *Pkhd1*, might be associated with the development of renal cysts in TAZ-deficient mice. Independently, Tian et al. (35) have reported that polycystin-2 is overexpressed in adult TAZ-deficient kidneys as a result of decreased ubiquitin-mediated degradation. In the present study, no changes in fibrocystin or polycystin-2 expression are observed in TAZ-deficient kidneys during the prenatal stage, when cyst formation starts. Abnormalities in fibrocystin and polycystin-2 may be involved in later stages of disease progression rather than initial cystogenesis.

Comparison of the renal phenotype of TAZ-deficient mice with human nephrogenic diabetes insipidus. A major difference between the renal phenotype of TAZ-deficient mice and human PKD is the presence of severely dilated calyces and massive polyuria. Although humans with ADPKD and ARPKD may have urinary concentration defects (6, 21), severe polyuria and hydronephrosis are not typical clinical features. TAZ-deficient mice have normal daily excretion of sodium and potassium, indicating that tubular electrolyte reabsorption is well preserved. The relatively low urine osmolality compared with wild-type together with impaired response to exogenous vasopressin are characteristic of nephrogenic diabetes insipidus. Hydronephrosis may be secondary to polyuria, as seen in congenital progressive hydronephrosis (*cph*) mutant mice (22). Thus the renal phenotype of TAZ-deficient mice is characterized by two distinct pathophysiological processes, cyst formation and urinary concentration defects.

Nephrogenic diabetes insipidus is caused by the inability of the renal collecting ducts to reabsorb water in response to vasopressin. About 90% of affected patients have mutations in the *AVPR2* gene, whereas the remaining 10% of patients are caused by *AQP2* gene mutations (28). However, TAZ-knockout kidneys do not show major abnormalities in the levels of expression of *Avpr2*, *Aqp2*, and *Aqp3*. In addition, the apical-basolateral polarity of aquaporin-2 and aquaporin-3 is preserved in both cystic and noncystic collecting ducts at embryonic and postnatal stages. These findings suggest that the polyuria and hydronephrosis in TAZ-deficient mice do not arise from major defects in the expression or localization of the V_2 vasopressin receptor, aquaporin-2, or aquaporin-3. Elucidation of the mechanism underlying the concentration defects in TAZ-deficient kidney may reveal novel pathways regulating renal water transport.

Possible requirement of TAZ for normal kidney development. The kidney develops through reciprocal interactions between the metanephric mesenchyme and the ureteric bud epithelium during embryogenesis (8, 36, 40). The ureteric bud grows into the metanephric mesenchyme and branches to form the collecting duct system while the mesenchyme adjacent to the tips of the ureteric bud is induced to condense and undergo a mesenchymal-to-epithelial transition. The resultant renal vesicle further differentiates into comma- and then S-shaped bodies. Morphogenesis and patterning of the epithelial structures lead to the formation and functional maturation of nephron segments including the glomerulus, the proximal tubule, the loop of Henle, and the distal tubule. Recent advances in gene targeting experiments have greatly contributed to the understanding of molecular mechanisms underlying the early "inductive" phase of kidney development. However, it remains largely unknown how each nephron segment is specified and functionally matures during the late phase of kidney development.

In situ hybridization and β-galactosidase staining demonstrated that *Taz* is diffusely expressed throughout the kidney. *Taz* expression is most intense in the nephrogenic zone during kidney development and is found in both mesenchymal and epithelial cells. *Taz* is not restricted to a specific segment of the nephron. Capillary endothelial cells also express *Taz*. *LacZ* expression is relatively scant and scattered compared with the pattern of in situ hybridization. This difference may be caused by deletion or disruption of critical enhancer element(s) during the generation of the targeted mutation.

In TAZ-deficient kidneys, most, but not all, of the cyst epithelium is *lacZ*-negative. In contrast, stromal cells, especially in the nephrogenic zone, show strong *lacZ* expression in TAZ-deficient kidneys. This finding indicates that TAZ may be crucial for gene expression in stromal cells supporting normal nephric development.

Pulmonary emphysematous changes in TAZ-deficient mice. In addition to renal cyst formation, TAZ-deficient mice demonstrate severely enlarged airspaces in the lung. This finding is morphologically reminiscent of human pulmonary emphysema, whose genetic pathogenesis is poorly understood. Only a congenital form of emphysema is known to be caused by a deficiency of α-antitrypsin, but its expression was not affected in TAZ-deficient mice (our unpublished data).

Pulmonary emphysema, as a manifestation of COPD, is regarded as a multifactorial disorder triggered by environmental factors such as cigarette smoking and pollutants. Although genetic factors involved in protease/antiprotease balance have been considered as possible determinants of susceptibility to emphysematous changes, the molecular pathogenesis is still unknown. In mice, emphysema-like pulmonary changes can be caused by deficiency in surfactant proteins SP-C or SP-D, possibly through increased activity of matrix metalloproteases (9, 38). Interestingly, TAZ has been reported to be a coactivator for the transcription factor TTF-1/Nkx2.1 and upregulates the expression of SP-C in respiratory epithelial cells (5). However, SP-C expression was not apparently affected in TAZ-deficient lungs (unpublished observations), so different mechanisms may generate the emphysematous changes in TAZ-deficient lungs.

The coexistence of renal and pulmonary abnormalities observed in TAZ-deficient mice has not been described before. However, there are similarities in the embryonic development of the kidney and lung. Both involve common processes, e.g., branching morphogenesis and common signaling pathways such as Shh, FGF, and BMP (17, 41). These similarities raise AQ: 7 the possibility that TAZ may be an effector in a common pathway that is involved in both lung and kidney development. Although the apical-basolateral polarity of epithelial cells in collecting ducts is not impaired in TAZ-deficient kidneys, further examination of the processes of epithelial tubule formation in TAZ-deficient kidneys and lungs may reveal a common mechanism for organogenesis and pathogenesis of human diseases.

ACKNOWLEDGMENTS

We thank Dr. Mark Knepper (National Heart, Lung, and Blood Institute) for the aquaporin-2 antibody.

GRANTS

This work was supported by Grants-in-Aid for Scientific Research from the Ministry of Education, Culture, Sports, Science, and Technology, Japan, Grants-in-Aid for Scientific Research from the Ministry of Health, Labour, and Welfare of Japan, a Research Grant from Uehara Memorial Foundation, the University of Texas Southwestern O'Brien Kidney Research Core Center (National Institute of Diabetes and Digestive and Kidney Diseases Grant P30DK-079328), and a Basil O'Connor Research Grant from the March of Dimes Birth Defects Foundation.

REFERENCES

1. **Barnes PJ.** New concepts in chronic obstructive pulmonary disease. *Annu Rev Med* 54: 113–129, 2003.
2. **Benezra R.** Polycystins: inhibiting the inhibitors. *Nat Cell Biol* 7: 1064–1065, 2005.
3. **Bisceglia M, Galliani CA, Senger C, Stallone C, Sessa A.** Renal cystic diseases: a review. *Adv Anat Pathol* 13: 26–56, 2006.
4. **Chen Q, Takahashi S, Zhong S, Hosoda C, Zheng HY, Ogushi T, Fujimura T, Ohta N, Tanoue A, Tsujimoto G, Kitamura T.** Function of the lower urinary tract in mice lacking alpha1d-adrenoceptor. *J Urol* 174: 370–374, 2005.
5. **Cui CB, Cooper LF, Yang X, Karsenty G, Aukhil I.** Transcriptional coactivation of bone-specific transcription factor Cbfa1 by TAZ. *Mol Cell Biol* 23: 1004–1013, 2003.
6. **D'Angelo A, Mioni G, Ossi E, Lupo A, Valvo E, Maschio G.** Alterations in renal tubular sodium and water transport in polycystic kidney disease. *Clin Nephrol* 3: 99–105, 1975.
7. **Deen PMT.** Mouse models for congenital nephrogenic diabetes insipidus: what can we learn from them? *Nephrol Dial Transplant* 22: 1023–1026, 2007.
8. **Dressler GR.** Tubulogenesis in the developing mammalian kidney. *Trends Cell Biol* 12: 390–395, 2002.
9. **Glasser SW, Detmer EA, Ikegami M, Na CL, Stahlman MT, Whitsett JA.** Pneumonitis and emphysema in sp-C gene targeted mice. *J Biol Chem* 278: 14291–14298, 2003.
10. **Guay-Woodford LM.** Murine models of polycystic kidney disease: molecular and therapeutic insights. *Am J Physiol Renal Physiol* 285: F1034–F1049, 2003.
11. **Gusmano R, Caridi G, Marini M, Perfumo F, Ghiggeri GM, Piaggio G, Ceccherini I, Seri M.** Glomerulocystic kidney disease in a family. *Nephrol Dial Transplant* 17: 813–818, 2002.
12. **Hogg JC.** Pathophysiology of airflow limitation in chronic obstructive pulmonary disease. *Lancet* 364: 709–721, 2004.
13. **Hong JH, Hwang ES, McManus MT, Amsterdam A, Tian Y, Kalmukova R, Mueller E, Benjamin T, Spiegelman BM, Sharp PA, Hopkins N, Yaffe MB.** TAZ, a transcriptional modulator of mesenchymal stem cell differentiation. *Science* 309: 1074–1078, 2005.
14. **Hong JH, Yaffe MB.** TAZ: a β-catenin-like molecule that regulates mesenchymal stem cell differentiation. *Cell Cycle* 5: 176–179, 2006.
15. **Horie S.** ADPKD: molecular characterization and quest for treatment. *Clin Exp Nephrol* 9: 282–291, 2005.
16. **Hossain Z, Ali SM, Ko HL, Xu J, Ng CP, Guo K, Qi Z, Ponniah S, Hong W, Hunziker W.** Glomerulocystic kidney disease in mice with a

targeted inactivation of Wwtr1. *Proc Natl Acad Sci USA* 104:1631–1636, 2007.

17. **Hu MC, Rosenblum ND.** Genetic regulation of branching morphogenesis: lessons learned from loss-of-function phenotypes. *Pediatr Res* 54: 433–438, 2003.
18. **Kanai F, Marignani PA, Sarbassova D, Yagi R, Hall RA, Donowitz M, Hisaminato A, Fujiwara T, Ito Y, Cantley LC, Yaffe MB.** TAZ: a novel transcriptional co-activator regulated by interactions with 14-3-3 and PDZ domain proteins. *EMBO J* 19: 6778–6791, 2000.
19. **Li X, Luo Y, Starremans PG, McNamara CA, Pei Y, Zhou J.** Polycystin-1 and polycystin-2 regulate the cell cycle through the helix-loop-helix inhibitor Id2. *Nat Cell Biol* 7: 1102–1112, 2005.
20. **Lu W, Peissel B, Babakhanlou H, Pavlova A, Geng L, Fan X, Larson C, Brent G, Zhou J.** Perinatal lethality with kidney and pancreas defects in mice with a targetted Pkd1 mutation. *Nat Genet* 17: 179–181, 1997.
21. **Martinez-Maldonado M, Yium JJ, Eknoyan G, Suki WN.** Adult polycystic kidney disease: studies of the defect in urine concentration. *Kidney Int* 2: 107–113, 1972.
22. **McDill BW, Li SZ, Kovach PA, Ding L, Chen F.** Congenital progressive hydronephrosis (cph) is caused by an S256L mutation in aquaporin-2 that affects its phosphorylation and apical membrane accumulation. *Proc Natl Acad Sci USA* 103: 6952–6957, 2006.
23. **Mochizuki T, Wu G, Hayashi T, Xenophontos SL, Veldhuisen B, Saris JJ, Reynolds DM, Cai Y, Gabow PA, Pierides A, Kimberling WJ, Breuning MH, Deltas CC, Peters DJ, Somlo S.** PKD2, a gene for polycystic kidney disease that encodes an integral membrane protein. *Science* 272: 1339–1342, 1996.
24. **Murakami M, Nakagawa M, Olson EN, Nakagawa O.** A WW domain protein TAZ is a critical coactivator for TBX5, a transcription factor implicated in Holt-Oram syndrome. *Proc Natl Acad Sci USA* 102: 18034–18039, 2005.
25. **Murakami M, Tominaga J, Makita R, Uchijima Y, Kurihara Y, Nakagawa O, Asano T, Kurihara H.** Transcriptional activity of Pax3 is co-activated by TAZ. *Biochem Biophys Res Commun* 339: 533–539, 2006.
26. **Nagy A, Gertsenstein M, Vintersten K, Behringer R.** *Manipulating the Mouse Embryo: A Laboratory Manual* (3rd ed.). Cold Spring Harbor, NY: Cold Spring Harbor Laboratory, 2003.
27. **Nakagawa O, Nakagawa M, Richardson JA, Olson EN, Srivastava D.** HRT1, HRT2, and HRT3: a new subclass of bHLH transcription factors marking specific cardiac, somitic, and pharyngeal arch segments. *Dev Biol* 216: 72–84, 1999.
28. **Nielsen S, Frøkiær J, Marples D, Kwon TH, Agre P, Knepper MA.** Aquaporins in the kidney: from molecules to medicine. *Physiol Rev* 82: 205–244, 2002.
29. **Onuchic LF, Furu L, Nagasawa Y, Hou X, Eggermann T, Ren Z, Bergmann C, Senderek J, Esquivel E, Zeltner R, Rudnik-Schoneborn S, Mrug M, Sweeney W, Avner ED, Zerres K, Guay-Woodford LM, Somlo S, Germino GG.** PKHD1, the polycystic kidney and hepatic disease 1 gene, encodes a novel large protein containing multiple immunoglobulin-like plexin-transcription-factor domains and parallel beta-helix 1 repeats. *Am J Hum Genet* 70: 1305–1317, 2002.
30. **Park KS, Whitsett JA, Di Palma T, Hong JH, Yaffe MB, Zannini M.** TAZ interacts with TTF-1 and regulates expression of surfactant protein-C. *J Biol Chem* 279: 17384–17390, 2004.
31. **Shao X, Johnson JE, Richardson JA, Hiesberger T, Igarashi P.** A minimal Ksp-cadherin promoter linked to a green fluorescent protein reporter gene exhibits tissue-specific expression in the developing kidney and genitourinary tract. *J Am Soc Nephrol* 13: 1824–1836, 2002.
32. **The European Polycystic Kidney Disease Consortium.** The polycystic kidney disease 1 gene encodes a 14 kb transcript and lies within a duplicated region on chromosome 16. *Cell* 77: 881–894, 1994.
33. **The International Polycystic Kidney Disease Consortium.** Polycystic kidney disease: the complete structure of the PKD1 gene and its protein. *Cell* 81: 289–298, 1995.
34. **Thurlbeck WM.** Measurement of pulmonary emphysema. *Am Rev Respir Dis* 95: 752–764, 1967.
35. **Tian Y, Kolb R, Hong JH, Carroll J, Li D, You J, Bronson R, Yaffe MB, Zhou J, Benjamin T.** TAZ promotes PC2 degradation through a $SCF^{\beta\text{-}Trcp}$ E3 ligase complex. *Mol Cell Biol* 27: 6383–6395, 2007.
36. **Vainio S, Lin Y.** Coordinating early kidney development: lessons from gene targeting. *Nat Rev Genet* 3: 533–543, 2002.
37. **Ward CJ, Hogan MC, Rossetti S, Walker D, Sneddon T, Wang X, Kubly V, Cunningham JM, Bacallao R, Ishibashi M, Milliner DS, Torres VE, Harris PC.** The gene mutated in autosomal recessive polycystic kidney disease encodes a large, receptor-like protein. *Nat Genet* 30: 259–269, 2002.
38. **Wert SE, Yoshida M, LeVine AM, Ikegami M, Jones T, Ross GF, Fisher JH, Korfhagen TR, Whitsett JA.** Increased metalloproteinase activity, oxidant production, and emphysema insurfactant protein D gene-inactivated mice. *Proc Natl Acad Sci USA* 97: 5972–5977, 2000.
39. **Witzgall R.** The proximal tubule phenotype and its disruption in acute renal failure and polycystic kidney disease. *Exp Nephrol* 7: 15–19, 1999.
40. **Yu J, McMahon AP, Valerius MT.** Recent genetic studies of mouse kidney development. *Curr Opin Genet Dev* 14: 550–557, 2004.
41. **Zegers MM, O'Brien LE, Yu W, Datta A, Mostov KE.** Epithelial polarity and tubulogenesis in vitro. *Trends Cell Biol* 13: 169–176, 2003.

JOBNAME: AUTHOR QUERIES PAGE: 1 SESS: 1 OUTPUT: Tue Jan 29 02:16:41 2008
/tapraid4/zh2-aflu/zh2-aflu/zh200308/zh25047d08z

AUTHOR QUERIES

AUTHOR PLEASE ANSWER ALL QUERIES

1

AQ1— Read proof, answer queries, and make corrections in margins. Return proof by overnight/express mail within 48 hours. Please e-mail (sdemma@the-aps.org) or fax (301-634-7243) answers to queries and a list of corrections before mailing. Please include the manuscript number in the subject line of your notification on all correspondence.

AQ2— Please note that the author list in the abstract line represents the form in which these names will appear in many online databases, such as the NCBI/NIH/NLM Pubmed database. Check this carefully, be sure there are no misrepresentations. Please make a note on the proof, if any corrections are needed.

AQ3— Please spell out NHERF.

AQ4— Please provide first initials and last names for all contributors to the unpublished observation by Amano et al.

AQ5— Please spell out FIAU and ICR.

AQ6— Simply writing that an experiment was done in accordance with certain guidelines is not sufficient. The protocol statement must indicate that the study was reviewed and approved. If the revised statement is not totally accurate, please make the necessary changes to correct it.

AQ8— Ed: Table and figures have been moved ahead of cite to avoid reference page.

AQ7— Please spell out FGF, BMP, and Shh.

AQ9— Ed: The side caption is deeper than the figure.

Am J Physiol Cell Physiol 292: C2141–C2149, 2007.
First published January 10, 2007; doi:10.1152/ajpcell.00295.2006.

β-Defensin overexpression induces progressive muscle degeneration in mice

Yasuhiro Yamaguchi,[1,3,4] Takahide Nagase,[2] Tetsuji Tomita,[1] Kyoko Nakamura,[4] Shigetomo Fukuhara,[4] Tomokazu Amano,[3] Hiroshi Yamamoto,[1] Yukie Ide,[5] Misao Suzuki,[6] Shinji Teramoto,[1] Tomoichiro Asano,[3] Kenji Kangawa,[7] Naomi Nakagata,[5] Yasuyoshi Ouchi,[1] and Hiroki Kurihara[3,4]

Departments of [1]Geriatric Medicine, [2]Respiratory Medicine, and [3]Physiological Chemistry and Metabolism, Graduate School of Medicine, The University of Tokyo, Bunkyo-ku, Tokyo; [4]Division of Integrative Cell Biology, Department of Embryogenesis, Institute of Molecular Embryology and Genetics, and Divisions of [5]Reproductive Engineering and [6]Transgenic Technology, Center for Animal Resources and Development, Kumamoto University, Kumamoto-shi, Kumamoto; and [7]Department of Biochemistry, National Cardiovascular Center Research Institute, Suita-ku, Osaka, Japan

Submitted 27 May 2006; accepted in final form 4 January 2007

Yamaguchi Y, Nagase T, Tomita T, Nakamura K, Fukuhara S, Amano T, Yamamoto H, Ide Y, Suzuki M, Teramoto S, Asano T, Kangawa K, Nakagata N, Ouchi Y, Kurihara H. β-Defensin overexpression induces progressive muscle degeneration in mice. *Am J Physiol Cell Physiol* 292: C2141–C2149, 2007. First published January 10, 2007; doi:10.1152/ajpcell.00295.2006.—Defensins comprise a family of cationic antimicrobial peptides characterized by conserved cysteine residues. They are produced in various organs including skeletal muscle and are identified as key elements in the host defense system as potent effectors. At the same time, defensins have potential roles in the regulation of inflammation and, furthermore, can exert cytotoxic effects on several mammalian cells. Here, we developed transgenic mice overexpressing mouse β-defensin-6 to explore the pathophysiological roles of the defensin family as a novel mediator of inflammatory tissue injury. Unexpectedly, the transgenic mice showed short lifespan, poor growth, and progressive myofiber degeneration with functional muscle impairment, predominant centronucleated myofibers, and elevated serum creatine kinase activity, as seen in human muscular dystrophy. Furthermore, some of the transgenic myofibers showed IκBα accumulation, which would be related to the myofiber apoptosis of limb-girdle muscular dystrophy type 2A. The present findings may unravel a concealed linkage between the innate immune system and the pathophysiology of degenerative diseases.

muscular dystrophy; innate immunity; NF-κB

ANTIMICROBIAL PEPTIDES have emerged as a part of the host defense mechanism in animals and plants (16, 29). Defensins comprise a family of mammalian cationic antimicrobial peptides, and α-, β-, and θ-defensin subfamily members exist that conserve three specific disulfide pairings. They are produced by leukocytes and various types of epithelial cells constitutively or in response to microbial signals and inflammatory cytokines (4, 9, 10, 14, 15).

While the immune response is indispensable for the survival of humans, the chronic inflammatory response is harmful and leads to various common disorders. In addition to the potent antimicrobial effects, defensins could act on diverse immune cells and epithelial cells through CCR6, Toll-like receptor-4 (TLR4), or other mechanisms, regulating the whole immune response (5, 23, 26, 37, 40, 41). Furthermore, they exert cytotoxic effects on mammalian cells themselves (18). α-Defensin causes cell lysis of variable cultured cells through the permeabilization of cell membrane (19) and subsequent DNA injury (11, 18). Although little information had been reported regarding β-defensin cytotoxicity (21, 23), treatment of mouse blastocysts with human β-defensin-2 (hBD-2) led to their degeneration and death (28). So some participation of the defensin family would be likely in the pathogenic immune response of various diseases (32).

Recently, we identified mouse β-defensin-6 (mBD-6), a β-defensin subfamily member expressed in skeletal muscle (39). mBD-6 expression was also augmented by bacterial endotoxin, perhaps under the regulation of the NF-κB pathway like hBD-2 and mouse β-defensin-3 (3). To explore the novel effects of this molecule, we generated transgenic mice overexpressing mBD-6 constitutively. Here, we show that the dysregulated β-defensin expression resulted in extensive myofiber degeneration, reminiscent of human muscular dystrophy.

Muscular dystrophy is an inherited disorder characterized by progressive muscle degeneration. The most common form, Duchenne muscular dystrophy, is caused by mutations in the dystrophin gene, and other causative molecules like dystroglycan and sarcoglycan organize dystrophin-glycoprotein complex binding to laminin (6, 17, 30). Another form of muscular dystrophy, limb-girdle muscular dystrophy type 2A (LGMD2A), has proved to be due to the defects of calpain-3, a proteolytic enzyme (24, 31, 35). While the identification of responsible genes for muscular dystrophy has improved, the pathogenic mechanisms are not clear enough to date. Multiple factors, including immune response, are related to the pathophysiology of muscular dystrophy (33). The present finding may give a clue to the novel involvement of innate immunity in degenerative diseases like muscular dystrophy.

MATERIALS AND METHODS

Generation of transgenic mouse. The transgene was constructed by inserting the mBD-6 cDNA 3′ downstream of the chicken β-actin promoter in the pCAGGS plasmid (a gift from J. Miyazaki) (22). The excised transgene was microinjected into fertilized C57BL6/J mouse oocytes. The genomic DNA was isolated from the mice tail and analyzed by Southern blotting and/or PCR. On Southern blot analysis, the genomic DNA was digested with *Bgl*II, resolved on 1.0% agarose gel, and transferred to the membrane. A 250-bp fragment containing the second exon of mBD-6 was labeled by [^{32}P]dCTP using a random primed DNA labeling kit (Roche). The labeled probe was hybrid-

Address for reprint requests and other correspondence: Y. Ouchi, Dept. of Geriatric Medicine, Graduate School of Medicine, The Univ. of Tokyo, 7-3-1 Hongo, Bunkyo-ku, Tokyo, 113-0033, Japan (e-mail: youchi-tky@umin.ac.jp).

The costs of publication of this article were defrayed in part by the payment of page charges. The article must therefore be hereby marked "*advertisement*" in accordance with 18 U.S.C. Section 1734 solely to indicate this fact.

ized to the membrane using ExpresHyb (Clontech). PCR was performed using the primers spanning mBD-6 cDNA (forward primer, 5′-GGTTATTGTGCTGTCTCATC-3′; reverse primer, 5′-ATTTGTGAGCCAGGGCATTG-3′). The PCR condition was 94°C for 40 s, 60°C for 30 s, and 72°C for 60 s, carried out for 35 cycles. The one line, Tg(CAG-mBD6)1 mice, was maintained on ICR mice, and the other line, Tg(CAG-mBD6)2 mice, was maintained on C57BL6/J mice. The immunohistochemical analysis was performed on Tg(CAG-mBD6)1 mice after they were backcrossed to the C57BL6/J strain. Animal care and use in our laboratory were in strict accordance with the guidelines for animal and recombinant DNA experiments put forth by Kumamoto University and The University of Tokyo. The experiment was approved by the Committee for Animal Resources in Kumamoto University and by the University of Tokyo.

RT-PCR. Total RNA was isolated from the skeletal muscle using ISOGEN (Nippon gene). Five micrograms of each sample were reverse-transcribed using SuperscriptII (Gibco-BRL). To detect the expression of transgene, we designed a forward primer from the mBD-6 first exon (5′-ACCATGAAGATCCATTACCTG-3′) and a reverse primer from the rabbit β-globin (5′-ATTTGTGAGCCAGGGCATTG-3′), and we performed a real-time PCR reaction using the Fluorescent Quantitative Detection System Version 3.02 (LineGene).

Antiserum preparation. The putative mature peptide composed of the COOH-terminal 40 amino acids of mBD-6 was chemically synthesized at the Peptide Institute (Minoh, Japan), as previously described (39). The anti-mBD-6 rabbit serum was prepared at the Peptide Institute using this synthetic mBD-6 peptide, conjugated to keyhole limpet hemocyanin, and injected into rabbits.

Isolation of mBD-6 peptide. We followed the procedure described by Valore et al. (36). Frozen skeletal muscle was homogenized in ISOGEN (Nippon gene), and the protein was extracted according to the manufacturer's protocol. Protein pellets were incubated overnight in 5% acetic acid at 4°C, and the dissolved proteins were neutralized with 10% NH_3. These protein solutions were separated on Tris-glycine SDS-PAGE and transferred onto polyvinylidene difluoride membrane. The membrane was probed with anti-mBD-6 rabbit serum, followed by a peroxidase-conjugated anti-rabbit IgG antibody (ICN), and visualized using the Enhanced Chemiluminescence Plus System (Amersham Pharmacia Biotech).

Evaluation of muscle strength. We evaluated muscle strength by measuring the time during which mice could hang down from a stainless steel lattice. The procedure was repeated twice for each mouse, and the better record was indicated.

Evans blue dye staining and measurement of serum creatine kinase activity. We performed the intraperitoneal injection of 10 mg/ml Evans blue dye solution of phosphate-buffered saline (PBS) (0.1 ml/10 g body wt) on 2-mo-old Tg1 mice and wild-type mice. The skeletal muscle samples were removed 16 h after the injection. The frozen 10-μm sections were fixed in acetone for 1 min and observed under a fluorescence microscope. Serum creatine kinase (CK) activity was measured at SRL (Tachikawa, Japan), a commercial laboratory.

Tissue preparation and immunohistochemistry. Skeletal muscle samples were removed and frozen in isopentane chilled in liquid nitrogen. The frozen 10-μm sections were processed for hematoxylin and eosin staining or immunohistochemical analysis. For the immunohistochemistry, the sections were fixed in acetone for 5 min and probed with the following primary antibodies: anti-dystrophin for COOH terminus (C-20) (Santa Cruz), anti-α-dystroglycan for internal core part (E-21) (Santa Cruz), anti-laminin-α2 chain (LSL), anti-neural cell adhesion molecule (Chemicon), anti-IκBα (Santa Cruz), anti-cleaved-caspase-3 (Trevigen), and anti-calpain-3 antibody (a gift from H. Sorimachi).

Statistics. Comparison of the body weights or serum CK activity was made with Student's *t*-test. Values of $P < 0.05$ were considered significant.

RESULTS

Generation of transgenic mice overexpressing mBD-6. To achieve broad and high expression of mBD-6, a cDNA fragment encoding mBD-6 was connected to the 3′-end of the chicken β-actin promoter flanked with a cytomegalovirus immediate-early enhancer (Fig. 1*A*). While six founder transgenic mice were identified using PCR and Southern blot analysis, the transgene was transmitted to germline in two lines. On Southern blot analysis, the one line, Tg(CAG-mBD6)1, was estimated to harbor several copies of the transgenes because of multiple extra bands, including a 2.0-kb DNA fragment corresponding to the full-length transgene size, while the wildtype genomic DNA showed two copies of the 1.4-kb intrinsic mBD-6 gene and a more faint 3.2-kb band perhaps composed

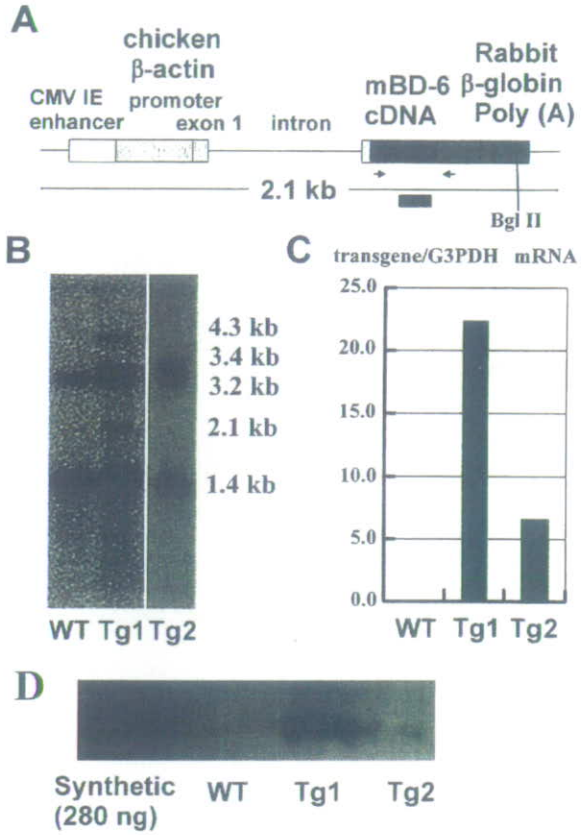

Fig. 1. Mouse β-defensin-6 (mBD-6) transgene expression. *A*: schematic description of the mBD-6 transgene fragment used to generate transgenic mice. A human cytomegalovirus immediate-early (CMV-IE) enhancer is linked to the chicken β-actin promoter, followed by its first exon and intron. In addition, a rabbit β-globin poly (A) sequence is located downstream from the mBD-6 cDNA. Black bar indicates probe of second exon of mBD-6 for Southern blot analysis in *B*. Arrows indicate the primers for RT-PCR of mBD-6 transgene. *B*: Southern blot analysis of the *Bgl*II-digested genomic DNA from Tg(CAGmBD6)1 mice (Tg1) and Tg(CAGmBD6)2 mice (Tg2). Wildtype genomic DNA showed two copies of the 1.4-kb intrinsic mBD-6 gene, and the more faint 3.2-kb band is perhaps composed of the mBD-6 pseudogene. Tg1 showed multiple extra bands, including a 2.1-kB DNA fragment corresponding to the full-length transgene size, while Tg2 showed a single 3.4-kb extra band. *C*: RT-PCR of mBD-6 transgene mRNA. The transgene-specific RT-PCR indicated transgene expression in skeletal muscle of Tg1 and Tg2. G3PDH, glyceraldehyde-3-phosphate dehydrogenase. *D*: Western blot analysis of mBD-6 peptide extracted from skeletal muscle; 280 ng of synthetic mBD-6 peptide composed of 40 NH_2-terminal residues were used as standard. mBD-6 peptide was detected in the extracts from Tg1 and Tg2 skeletal muscle but not from the wild-type mice (WT).

of the mBD-6 pseudogene. The other line, Tg(CAG-mBD6)2, was estimated to harbor a single copy because of the single 3.4-kb extra band (Fig. 1*B*). Tg(CAG-mBD6)1 and Tg(CAG-mBD6)2 mice will be referred to as Tg1 mice and Tg2 mice, respectively.

In both lines, transgene expression was detected in the skeletal muscle by RT-PCR using the primers from mBD-6 cDNA and rabbit β-globin cDNA (Fig. 1, *A* and *B*). Tg1 mice showed 3.4 times higher expression of the transgene than Tg2 mice. Western blot analysis could detect mBD-6 peptide in the extracts from Tg1 and Tg2 skeletal muscle, and the expression level was also low in Tg2 mice (Fig. 1*C*). In wild-type mice, the mBD-6 signal was not detected by Western blot analysis under the same experimental condition. Immunohistochemical analysis of the mBD-6 peptide showed the mBD-6 peptide stored in the cytoplasmic granules in some skeletal muscle myofibers of Tg1 mice.

Tg(CAG-mBD6) mice develop muscle degeneration. At birth, Tg1 and Tg2 mice were indistinguishable from their wild-type littermates. By 6 wk of age, poor growth of Tg1 mice became evident, and at 8 wk of age, both the male and female body weights of Tg1 mice were significantly lower than those of their wild-type littermates ($P < 0.01$) (Fig. 2*A*). The mean body weight of Tg1 mice was ~80% that of their wildtype littermates. They showed contracted stiff limbs and progressive kyphosis by 6 mo of age (Fig. 2*B*). Most of Tg1 mice died before 11 mo of age. The short lifespan of Tg1 mice was more evident after they were backcrossed to the C57BL6/J strain. Many of the Tg1 mice died before 8 mo, and no mice backcrossed to the C57BL6/J strain lived for >1 yr. We could not clarify the specific cause of Tg1 mouse death except severe loss of body weight. Although the other transgenic line, Tg2, did not reveal so prominently poor growth or kyphosis, 6-mo-old Tg2 male mice also showed significantly lower body weights than wild-type littermates. Tg2 mice lived for >12 mo.

Regarding the decreased body weight, we evaluated the food intake of 5-wk-old Tg1 mice. The food intake of Tg1 mice was 3.31 ± 0.12 g/day, which was significantly lower than the food intake of the wild-type littermates, which was 4.00 ± 0.29 g/day ($P < 0.05$).

Because progressive kyphosis is a prominent feature caused by functional impairment of skeletal muscle, we evaluated the muscle strength of Tg1 mice by hanging them from a stainless steel lattice. Two-month-old Tg1 mice dropped in a significantly shorter time from the lattice, indicating muscle weakness in Tg1 mice. While most of the wild-type littermates hung for >120 s, significantly more Tg1 mice dropped before 60 s ($P < 0.01$) (Fig. 3).

Hematoxylin and eosin staining of skeletal muscle revealed degenerative myofibers, infiltration of mononuclear cells, and some centronucleated myofibers in 4-wk-old Tg1 mice. After 8 wk of age, centronucleated myofibers became much more predominant, and faintly stained necrotic myofibers, basophilic regenerating myofibers, and fiber splitting were frequently encountered. The myofibers also showed prominent differences in size (Fig. 3). These features were observed in all skeletal muscles examined, including gastrocnemius muscles, anterior tibial muscles, soleus muscles, diaphragm, and muscles of the back. Meanwhile, no histological abnormalities were noted in 20-day-old Tg1 mice (Fig. 4). The other transgenic line, Tg2, revealed no histological abnormalities in skeletal muscle until ~6 mo of age. However, 1-yr-old Tg2 mice showed a few faintly stained degenerative myofibers in various muscles. The number of centronucleated myofibers in 1-yr-old Tg2 mice was also significantly increased compared with wild-type mice of the same age (2.5 ± 0.5 vs. 0.2 ± 0.1%).

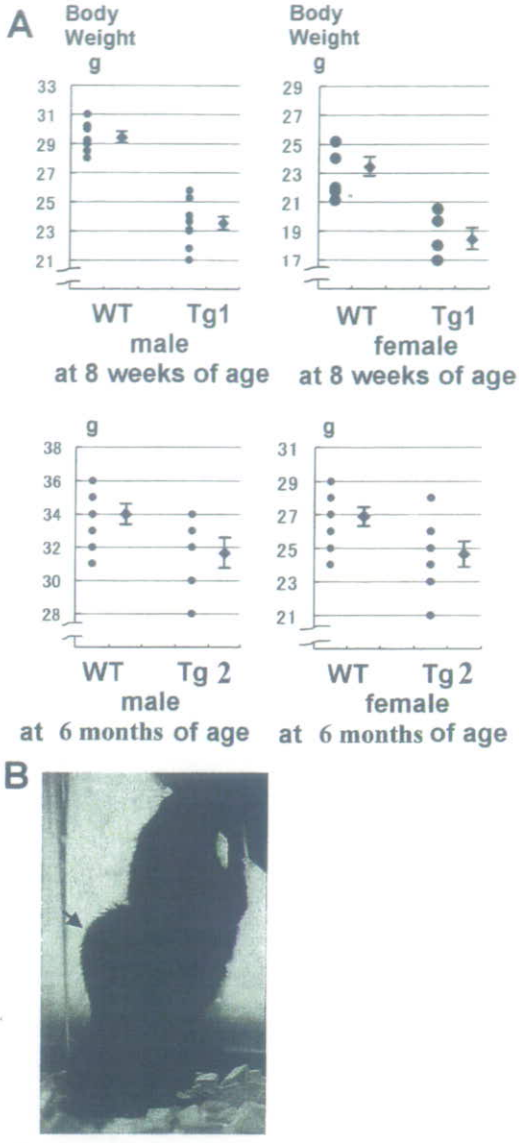

Fig. 2. Poor growth and progressive kyphosis of Tg1 mice. *A*: comparison of body weights between Tg and WT mice. Each circular point (●) indicates the measured individual body weight. Mean values (◆) ± SD are also shown. Both the male and female body weights of Tg mice were significantly lower than those of WT. *B*: photograph of 6-mo-old Tg1 mouse. Arrow indicates kyphosis.

We measured serum CK activity in 3-mo-old Tg-1 mice and their wild-type littermates because the measurement of serum CK activity is used clinically to ascertain muscular damage. Tg1 mice showed significantly higher serum CK activity than the wild-type littermates ($P < 0.01$) (Fig. 5*A*). Evans blue dye labeling also detected more clearly the damaged myofibers, with increased membrane permeability in Tg1 mice and aged 1-yr-old Tg2 mice (Fig. 5*B*).

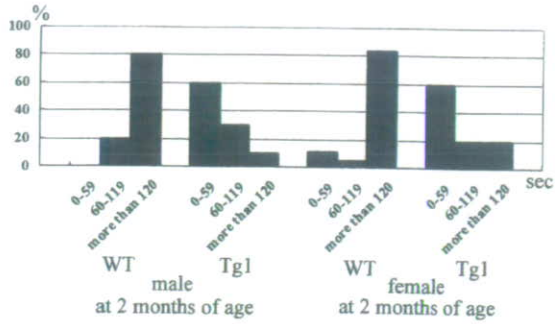

Fig. 3. Evaluation of muscle strength of Tg1 mice. We evaluated muscle strength by measuring the time during which mice could hang down from a stainless steel lattice. Graph shows percentage of mice that could hang down for the indicated time. While most of the WT littermates hung down for >120 s, many of Tg1 mice dropped before 60 s.

Evaluation of causative proteins of muscular dystrophy. These skeletal muscle phenotypes caused by mBD-6 overexpression are reminiscent of muscular dystrophies, characterized by progressive myofiber degeneration. In mBD-6 transgenic mice, organization of the dystrophin-glycoprotein complex was not different from that of wild-type littermates on the immunohistochemistry of dystrophin, α-dystroglycan, and laminin (Fig. 6). Likewise, the expression of calpain-3 showed no abnormality in mBD-6 transgenic mice (Fig. 6).

Immunohistochemical abnormalities of the transgenic myofibers. To investigate the molecular mechanisms of myofiber degeneration, we evaluated the conserved immunohistochemical features of young Tg1 mice and aged Tg2 mice.

In 1-mo-old Tg1 mice, many myofibers showed a high level of expression of neural cell adhesion molecule (NCAM). Also, in Tg2 mice, many NCAM-positive myofibers were detected at 11–12 mo of age, while their wild-type littermates of the same age showed only a few NCAM-positive myofibers (Fig. 7*A*). Although denervated myofibers upregulate NCAM expression, the number and morphology of motor neurons were not different between the Tg1 mice and their wild-type littermates (Fig. 8). We also examined the distribution of IκBα in Tg1 and Tg2 mice. We detected the accumulation of IκBα in many myofibers of 1-mo-old Tg1 mice and 12-mo-old Tg2 mice (Fig. 7*B*), as reported in LGMD2A patients (2). We also evaluated the apoptotic features of IκBα-positive myofibers in transgenic mice. In the staining of serial sections, some of the IκBα-positive myofibers showed the signal of cleaved caspase-3, the active form of caspase-3, indicating activation of the apoptotic pathway (Fig. 9).

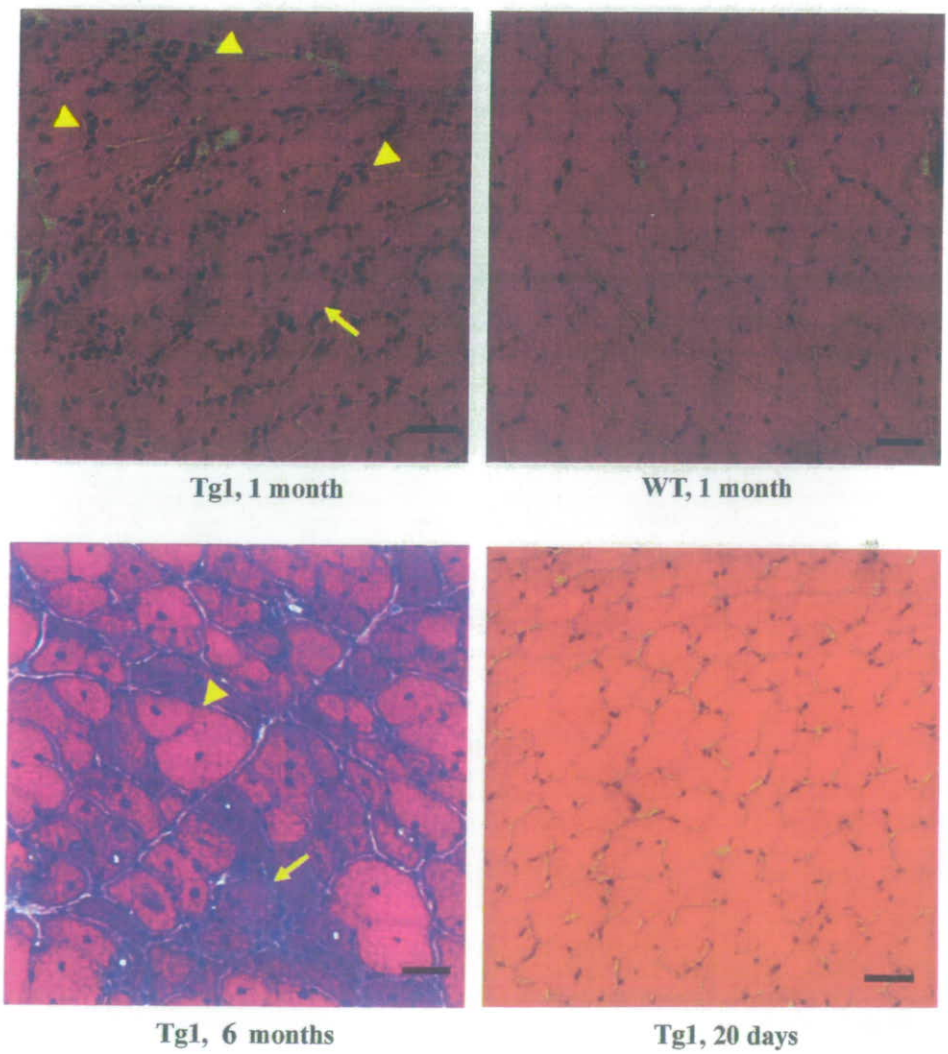

Fig. 4. Progressive myofiber degeneration of Tg1 mice. Hematoxylin and eosin staining of gastrocnemius muscles of Tg1 mice at the age of 20 days, 1 mo, and 6 mo. At the age of 1 mo, faintly stained degenerative myofibers (arrow) and centronucleated myofibers appeared in the Tg1 mouse, in contrast to the WT littermate. Arrowheads indicate the infiltration of mononuclear cells. At the age of 6 mo, centronucleated myofibers were more predominant, with prominent differences in size. Fiber splitting (arrowhead) is also indicated. No histological abnormalities were noted at the age of 20 days. Scale bars: 40 μm.

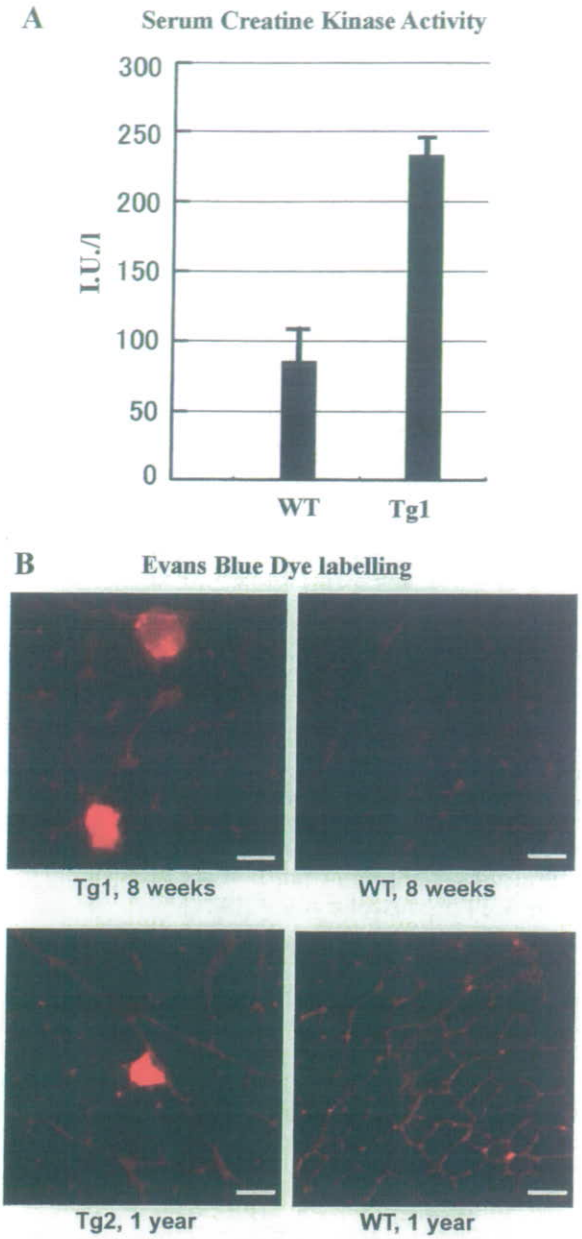

Fig. 5. Evaluation of membrane permeability of Tg1 skeletal muscle. *A*: serum creatine kinase (CK) activity of Tg1 mice at the age of 3 mo. Tg1 mice showed significantly higher CK activity than WT littermates ($P < 0.01$). *B*: after Evans blue dye injections, some myofibers of Tg1 mice and 1-yr-old Tg2 mice accumulated the dye in cytoplasm, showing increased membrane permeability. Scale bars: 40 μm.

Other pathological changes and food intake in the mBD-6 overexpressing mouse. mBD-6 overexpression decreases body weights and increases centronucleated myofibers and degenerative myofibers in mice. Kyphosis of vertebra, shortness in height, and slow movement were observed in the mouse. The food intake of Tg1 mice was significantly lower than that of the wild-type littermates. The short lifespan of Tg1 mice was evident, especially after they were backcrossed to the C57BL6/J strain. Many Tg1 mice died before 8 mo, and no mice backcrossed to the C57BL6/J strain lived for >1 yr. There was no evidence of cancer in the dead Tg1 mice.

DISCUSSION

Our data first demonstrated the pathogenic effects of dysregulated β-defensin expression in vivo. Western blot analysis of muscle extracts ascertained the overproduction of mature mBD-6 peptide in the Tg1 and Tg2 mice. The dysregulated β-defensin expression induced poor growth, short lifespan, and functional muscle impairment. Pathologically, the skeletal muscle of Tg1 mice showed progressive degeneration and regeneration of myofibers, consistent with the histology of muscular dystrophy. Elevated serum CK activity and positive Evans blue dye labeling in Tg1 mice indicated the disruption of the myofiber plasma membrane, also consistent with muscular dystrophy.

Despite recent identification of causative genes, the clinical course of muscular dystrophy is miserable lacking an established therapy. Although gene therapy could be curative, replacing the ultimate defect, many obstacles exist to technical progress. So, presently, important therapy targets are the factors modulating the state of muscle degeneration. Clinically,

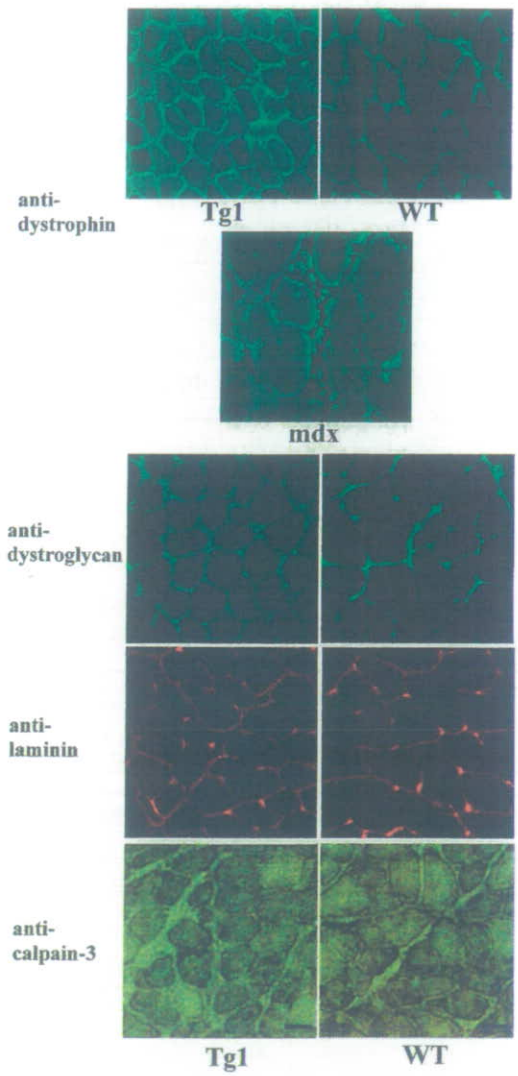

Fig. 6. Immunohistochemical analyses of dystrophin, α-dystroglycan, laminin, and calpain-3 distributions in Tg1 skeletal muscle. Distribution of these molecules in Tg1 mice showed no difference from WT. Dystrophin is absent in dystrophin-deficient muscle (mdx). Scale bars: 20 μm.

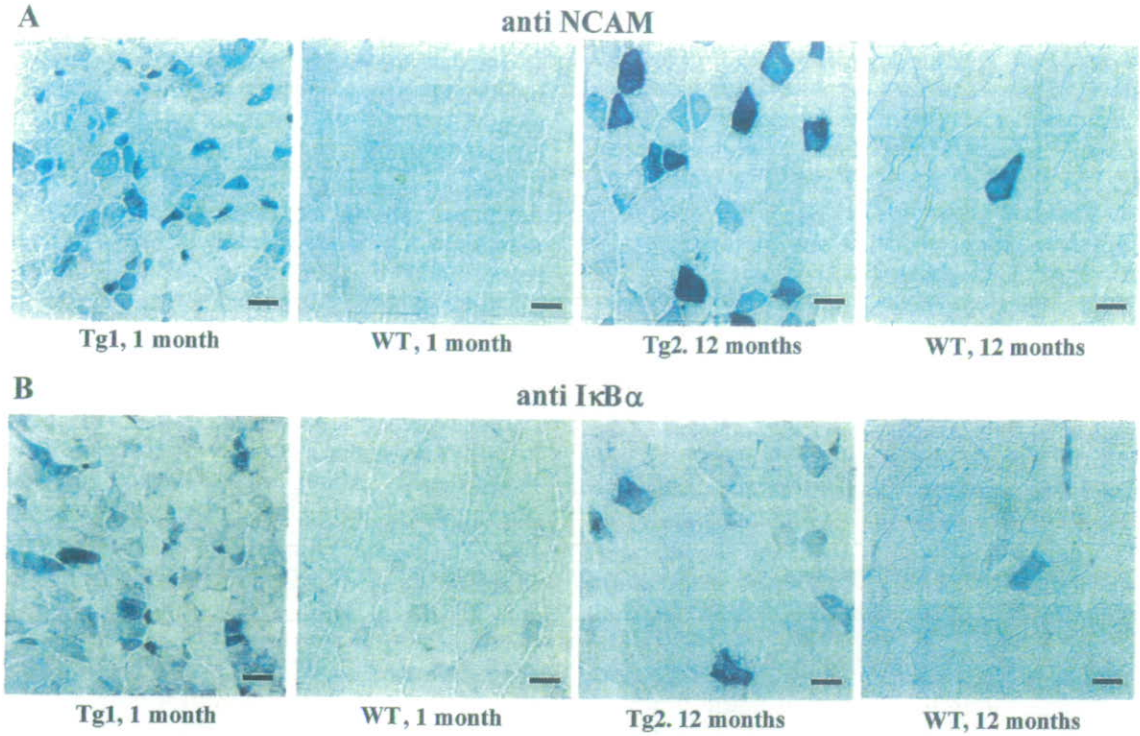

Fig. 7. Immunohistochemical analyses of neural cell adhesion molecule (NCAM) and IκBα distributions in young Tg1 mice and aged Tg2 mice. *A*: many myofibers showed a high level of expression of NCAM in 1-mo-old Tg1 mice and 12-mo-old Tg2 mice, in contrast to WT littermates. *B*: many myofibers showed accumulation of IκBα in 1-mo-old Tg1 mice and 12-mo-old Tg2 mice, in contrast to WT littermates. Scale bars: 40 μm.

glucocorticoids are utilized to delay the progression of Duchene muscular dystrophy (12, 20, 34), and, actually, the invasion of lymphoid and myeloid cells is an early stage feature of Duchene muscular dystrophy (33). β-Defensin would be the first reported component of inflammation that induced alone the typical phenotype of muscular dystrophy. Because mBD-6 and human defensin-3 showed intrinsic expression in skeletal muscle (10, 39), and invaded myeloid cells and lymphocytes would secrete abundant α-defensin in human muscular dystrophy (42), our findings suggest the significance of the defensin family in the pathogenesis of muscular dystrophy.

In aged Tg2 mice, mBD-6 overexpression induced NCAM-positive myofibers and IκBα accumulation with mild histological abnormality. Interestingly, aging alone induced a slight increase in NCAM-positive myofibers and IκBα-positive myofibers. The augmentation of these aging phenomena in Tg2 mice suggested that defensin-mediated muscle degeneration would not be limited to distinct muscular dystrophy but would

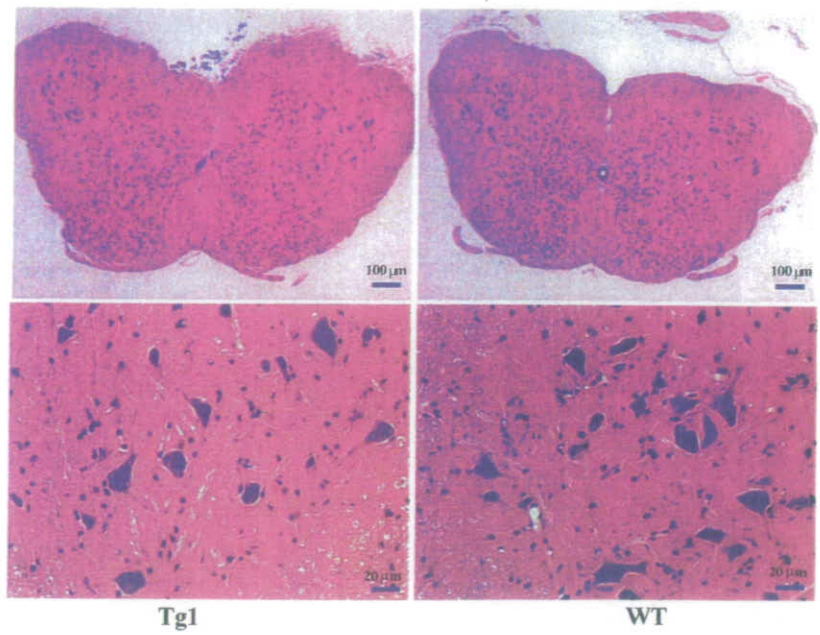

Fig. 8. Hematoxylin and eosin staining of spinal cords of Tg1 mouse and WT littermate. No. and morphology of motor neurons showed no abnormality causative of myofiber degeneration in the Tg1 mouse.

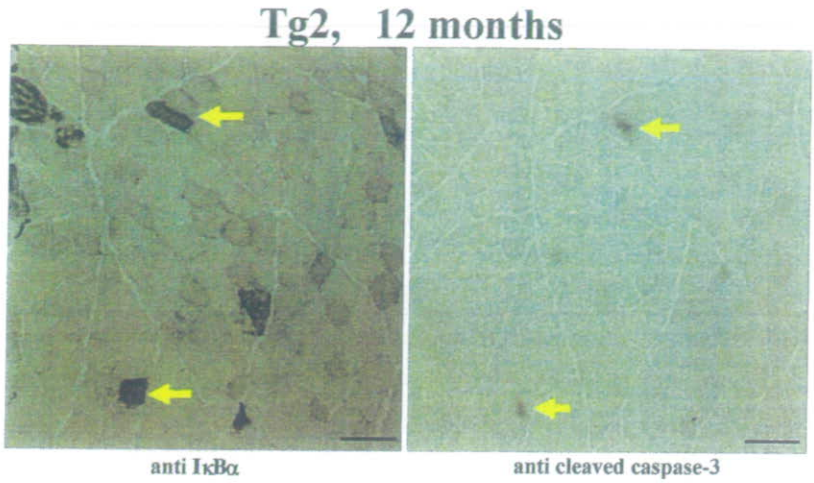

Fig. 9. Apoptotic feature of Tg2 skeletal muscle. Immunohistochemical analysis of serial sections for IκBα and cleaved caspase-3 indicated that some myofibers (arrow) showed both accumulation of IκBα and apoptotic features. Scale bars: 40 μm.

be associated with a much more common late-onset muscular wasting degeneration like sarcopenia, cachexia, or senescence acceleration.

Previous studies with transgenic mice overexpressing antimicrobial proteins (e.g., lysozyme) or peptides (e.g., human defensin-5) have indicated the beneficial roles of these substances in the in vivo situation (1, 27). In contrast to these animal models, Tg1 mice succumbed to muscular degeneration and short lifespan, showing a completely novel aspect of antimicrobial peptides. The various mediators, like reactive oxygen metabolites, complement cascades, and some proteases are involved in the known immune-mediated tissue injury in inflammatory conditions. Our investigation has established the defensin family as a novel effector of immune-mediated tissue injury.

The molecular mechanism of defensin-mediated tissue injury remains to be clarified. Generally, pore formation and permeabilization of target membranes are common mechanisms of defensin effects (9, 18, 19). Because dystrophin, dystroglycan, and laminin distributions were normal, mBD-6 would induce muscle degeneration independently of the dystrophin-glycoprotein complex.

Although upregulation of NCAM was shown in denervated myofibers, the histology of motor neurons of Tg1 mice showed no abnormality that could be causative for massive myofiber degeneration. So, these NCAM-positive myofibers would indicate the regenerative process and/or association of motor endplate degeneration in Tg1 and Tg2 mice, as indicated in some types of muscular dystrophy (7, 13, 38). At the same time, the accumulation of IκBα in Tg1 and Tg2 mice with apoptotic features is similar to that in LGMD2A patients and their animal models (2, 25). In LGMD2A patients, the defect of IκBα turnover inhibited the activity of NF-κB, associated with myofiber apoptosis. Because perturbation of the NF-κB/IκB pathway could cause the subsequent perturbation of many survival genes, it could be a common pathway in various mechanisms of myofiber degeneration.

The next question is, what downstream events of the β-defensin-6 pathway might be involved in the mechanisms of myofiber degeneration? Actually, both CCR6 and TLR4 are expressed in skeletal muscle. Other investigators (8) have reported that TLR4 expression is identified in skeletal muscles. We also confirmed the expression of TLR4 using RT-PCR. However, we do not think that the downstream events of the β-defensin-6 pathway are important in the pathogenesis of the muscle degeneration phenotype. Until now, there have been no data about the pathological relationship between muscle degeneration and TLRs. While various functions of the defensin family in mammalian cells have been reported, including cytotoxicity, most of the downstream events were not clarified, and the contribution of CCR6 or TLR4 on the pathogenesis of muscle degeneration would be limited, if it existed. Certainly, CCR6 receptors and TLR4 are expressed in skeletal muscle, and the NF-κB pathway is directly associated with TLR4. However, it is reasonable to speculate that continuous stimulation of these receptors does not primarily contribute to induce degeneration of myofibers in vivo. If such a phenomenon were to happen, the muscles could be totally abolished, and severe muscle damage would occur earlier in life.

In this study, body weights of Tg1 mice were significantly lower than for wild-type mice. Food intake of Tg1 mice was significantly lower than for wild-type littermates. The decreased food intake could explain, in part, decreased body weight. However, prominent myofiber degeneration could never be induced by decreased food intake, and it is more likely that decreased food intake resulted from decreased muscular mass and strength. Furthermore, Tg1 mice had a short life span. Most Tg1 mice died before 11 mo of age. The short lifespan of Tg1 mice was especially evident after they were backcrossed to the C57Bl6/J strain. Many Tg1 mice died before 8 mo, and no mice backcrossed to the C57BL6/J strain lived for >1 yr. We could not clarify the specific cause of Tg1 mouse death except severe loss of body weight. There was no evidence of cancer in the dead Tg1 mice; thus we speculate that impaired immune function may cause systemic inflammation and decreased food intake at a relatively young age, resulting in a malnutrition-related short lifespan.

In conclusion, our study has demonstrated that the defensin family could contribute to the pathogenic immune response in animal models, especially in the pathogenesis of myofiber degeneration.

ACKNOWLEDGMENTS

We thank H. Sugita and I. Nonaka for helpful discussion. We also thank H. Sorimachi for providing calpain-3 antibody and J. Miyazaki for the pCAGGS plasmid.

GRANTS

This work was supported in part by Grants-in-Aid for Scientific Research from the Ministry of Education, Science, Sports and Culture of Japan, Grants-in-Aid for Comprehensive Research on Aging and Health from the Ministry of Health, Labor and Welfare of Japan, and a Research Grant from Uehara Memorial Foundation.

REFERENCES

1. **Akinbi HT, Epaud R, Bhatt H, Weaver TE.** Bacterial killing is enhanced by expression of lysozyme in the lungs of transgenic mice. *J Immunol* 165: 5760–5766, 2000.
2. **Baghdiguian S, Martin M, Richard I, Pons F, Astier C, Bourg N, Hay RT, Chemaly R, Halaby G, Loiselet J, Anderson LV, Lopez de Munain A, Fardeau M, Mangeat P, Beckmann JS, Lefranc G.** Calpain 3 deficiency is associated with myonuclear apoptosis and profound perturbation of the IkappaB alpha/NF-kappaB pathway in limb-girdle muscular dystrophy type 2A. *Nat Med* 5: 503–511, 1999.
3. **Bals R, Wang X, Meegalla RL, Wattler S, Weiner DJ, Nehls MC, Wilson JM.** Mouse beta-defensin 3 is an inducible antimicrobial peptide expressed in the epithelia of multiple organs. *Infect Immun* 67: 3542–3547, 1999.
4. **Becker MN, Diamond G, Verghese MW, Randell SH.** CD14-dependent lipopolysaccharide-induced beta-defensin-2 expression in human tracheobronchial epithelium. *J Biol Chem* 275: 29731–29736, 2000.
5. **Biragyn A, Ruffini PA, Leifer CA, Klyushnenkova E, Shakhov A, Chertov O, Shirakawa AK, Farber JM, Segal DM, Oppenheim JJ, Kwak LW.** Toll-like receptor 4-dependent activation of dendritic cells by beta-defensin 2. *Science* 298: 1025–1029, 2002.
6. **Dalkilic I, Kunkel LM.** Muscular dystrophies: genes to pathogenesis. *Curr Opin Genet Dev* 13: 231–238, 2003.
7. **Deconinck AE, Rafael JA, Skinner JA, Brown SC, Potter SC, Metzinger L, Watt DJ, Dickson JG, Tinsley JM, Devies KE.** Utrophin-dystrophin-deficient mice as a model for Duchenne muscular dystrophy. *Cell* 90: 717–727, 1997.
8. **Frost RA, Nystrom GJ, Lang CH.** Lipopolysaccharide stimulates nitric oxide synthase-2 expression in murine skeletal muscle and C(2)C(12) myoblasts via Toll-like receptor-4 and c-Jun NH(2)-terminal kinase pathways. *Am J Physiol Cell Physiol* 287: C1605–C1615, 2004.
9. **Ganz T.** Defensins: antimicrobial peptides of innate immunity. *Nat Rev Immunol* 3: 710–720, 2003.
10. **Garcia JR, Jaumann F, Schulz S, Krause A, Rodriguez-Jimenez J, Forssmann U, Adermann K, Kluver E, Vogelmeier C, Becker D, Hedrich R, Forssmann WG, Bals R.** Identification of a novel, multifunctional beta-defensin (human beta-defensin 3) with specific antimicrobial activity. Its interaction with plasma membranes of Xenopus oocytes and the induction of macrophage chemoattraction. *Cell Tissue Res* 306: 257–264, 2001.
11. **Gera JF, Lichtenstein A.** Human neutrophil peptide defensins induce single strand DNA breaks in target cells. *Cell Immunol* 138: 108–120, 1991.
12. **Gosselin LE, McCormick KM.** Targeting the immune system to improve ventilatory function in muscular dystrophy. *Med Sci Sports Exerc* 36: 44–51, 2004.
13. **Grady RM, Akaaboune M, Cohen AL, Maimone MM, Lichtman JW, Sanes JR.** Tyrosine-phosphorylated and nonphosphorylated isoforms of alpha-dystrobrevin: roles in skeletal muscle and its neuromuscular and myotendinous junctions. *J Cell Biol* 160: 741–752, 2003.
14. **Harder J, Bartels J, Christophers E, Schröder JM.** A peptide antibiotic from human skin. *Nature* 387: 861, 1997.
15. **Harder J, Bartels J, Christophers E, Schröder JM.** Isolation and characterization of human beta-defensin-3, a novel human inducible peptide antibiotic. *J Biol Chem* 276: 5707–5713, 2001.
16. **Hoffmann JA, Kafatos FC, Janeway CA, Ezekowitz RA.** Phylogenetic perspectives in innate immunity. *Science* 284: 1313–1318, 1999.
17. **Laval SH, Bushby KM.** Limb-girdle muscular dystrophies–from genetics to molecular pathology. *Neuropathol Appl Neurobiol* 30: 91–105, 2004.
18. **Lehrer RI, Lichtenstein AK, Ganz T.** Defensins: antimicrobial and cytotoxic peptides of mammalian cells. *Annu Rev Immunol* 11: 105–128, 1993.
19. **Lichtenstein A.** Mechanism of mammalian cell lysis mediated by peptide defensins. Evidence for an initial alteration of the plasma membrane. *J Clin Invest* 88: 93–100, 1991.
20. **Mendell JR, Moxley RT, Griggs RC, Brooke MH, Fenichel GM, Miller JP, King W, Signore L, Pandya S, Florence J.** Randomized, double-blind six-month trial of prednisone in Duchenne's muscular dystrophy. *N Engl J Med* 320: 1592–1597, 1989.
21. **Nishimura M, Abiko Y, Kurashige Y, Takeshima M, Yamazaki M, Kusano K, Saitoh M, Nakashima K, Inoue T, Kaku T.** Effect of defensin peptides on eukaryotic cells: primary epithelial cells, fibroblasts and squamous cell carcinoma cell lines. *J Dermatol Sci* 36: 87–95, 2004.
22. **Niwa H, Yamamura K, Miyazaki J.** Efficient selection for high-expression transfectants with a novel eukaryotic vector. *Gene* 108: 193–200, 1991.
23. **Niyonsaba F, Ushio H, Nagaoka I, Okumura K, Ogawa H.** The human beta-defensins (-1, -2, -3, -4) and cathelicidin LL-37 induce IL-18 secretion through p38 and ERK MAPK activation in primary human keratinocytes. *J Immunol* 175: 1776–1784, 2005.
24. **Richard I, Broux O, Allamand V, Fougerousse F, Chiannilkulchai N, Bourg N, Brenguier L, Devaud C, Pasturaud P, Roudaut C, Hillaire D, Passos-Bueno MR, Zatz M, Tischfield JA, Fardeau M, Jackson CE, Cohen D, Beckmann JS.** Mutations in the proteolytic enzyme calpain 3 cause limb-girdle muscular dystrophy type 2A. *Cell* 7: 27–40, 1995.
25. **Richard I, Roudaut C, Marchand S, Baghdiguian S, Herasse M, Stockholm D, Ono Y, Suel L, Bourg N, Sorimachi H, Lefranc G, Fardeau M, Sebille A, Beckmann JS.** Loss of calpain 3 proteolytic activity leads to muscular dystrophy and to apoptosis-associated IkappaBalpha/nuclear factor kappaB pathway perturbation in mice. *J Cell Biol* 151: 1583–1590, 2000.
26. **Sakamoto N, Mukae H, Fujii T, Ishii H, Yoshioka S, Kakugawa T, Sugiyama K, Mizuta Y, Kadota J, Nakazato M, Kohno S.** Differential effects of alpha- and beta-defensin on cytokine production by cultured human bronchial epithelial cells. *Am J Physiol Lung Cell Mol Physiol* 288: L508–L513, 2005.
27. **Salzman NH, Ghosh D, Huttner KM, Paterson Y, Bevins CL.** Protection against enteric salmonellosis in transgenic mice expressing a human intestinal defensin. *Nature* 422: 522–526, 2003.
28. **Sawicki W, Mystkowska ET.** Contraceptive potential of peptide antibiotics. *Lancet* 353: 464–465, 1999.
29. **Schröder JM.** Epithelial antimicrobial peptides innate local host response elements. *Cell Mol Life Sci* 56: 32–46, 1999.
30. **Spence HJ, Chen YJ, Winder SJ.** Muscular dystrophies, the cytoskeleton and cell adhesion. *Bioessays* 24: 542–552, 2002.
31. **Spencer MJ, Guyon JR, Sorimachi H, Potts A, Richard I, Herasse M, Chamberlain J, Dalkilic I, Kunkel LM, Beckmann JS.** Stable expression of calpain 3 from a muscle transgene in vivo: immature muscle in transgenic mice suggests a role for calpain 3 in muscle maturation. *Proc Natl Acad Sci USA* 99: 8874–8879, 2002.
32. **Spencer LT, Paone G, Krein PM, Rouhani FN, Rivera-Nieves J, Brantly ML.** Role of human neutrophil peptides in lung inflammation associated with alpha1-antitrypsin deficiency. *Am J Physiol Lung Cell Mol Physiol* 286: L514–L520, 2004.
33. **Spencer MJ, Tidball JG.** Do immune cells promote the pathology of dystrophin-deficient myopathies? *Neuromuscul Disord* 11: 556–564, 2001.
34. **St-Pierre SJ, Chakkalakal JV, Kolodziejczyk SM, Knudson JC, Jasmin BJ, Megeney LA.** Glucocorticoid treatment alleviates dystrophic myofiber pathology by activation of the calcineurin/NF-AT pathway. *FASEB J* 18: 1937–1939, 2004.
35. **Tagawa K, Taya C, Hayashi Y, Nakagawa M, Ono Y, Fukuda R, Karasuyama H, Toyama-Sorimachi N, Katsui Y, Hata S, Ishiura S, Nonaka I, Seyama Y, Arahata K, Yonekawa H, Sorimachi H, Suzuki K.** Myopathy phenotype of transgenic mice expressing active site-mutated inactive p94 skeletal muscle-specific calpain, the gene product responsible for limb girdle muscular dystrophy type 2A. *Hum Mol Genet* 9: 1393–1402, 2000.
36. **Valore EV, Park CH, Quayle AJ, Wiles KR, McCray PB Jr, Ganz T.** Human beta-defensin-1: an antimicrobial peptide of urogenital tissues. *J Clin Invest* 101: 1633–1642, 1998.
37. **Van Wetering S, Sterk PJ, Rabe KF, Hiemstra PS.** Defensins: key players or bystanders in infection, injury, and repair in the lung? *J Allergy Clin Immunol* 104: 1131–1138, 1999.
38. **Winter A, Bornemann A.** NCAM, vimentin and neonatal myosin heavy chain expression in human muscle diseases. *Neuropathol Appl Neurobiol* 25: 417–424, 1999.
39. **Yamaguchi Y, Fukuhara S, Nagase T, Tomita T, Hitomi S, Kimura S, Kurihara H, Ouchi Y.** A novel mouse β-defensin, mBD-6, predomi-

nantly expressed in skeletal muscle. *J Biol Chem* 276: 31510–31514, 2001.

40. **Yang D, Biragyn A, Kwak LW, Oppenheim JJ.** Mammalian defensins in immunity: more than just microbicidal. *Trends Immunol* 23: 291–296, 2002.
41. **Yang D, Chertov O, Bykovskaia SN, Chen Q, Buffo MJ, Shogan J, Anderson M, Schröder JM, Wang JM, Howard OM, Oppenheim JJ.** Beta-defensins: linking innate and adaptive immunity through dendritic and T cell CCR6. *Science* 286: 525–528, 1999.
42. **Zhang L, Yu W, He T, Yu J, Caffrey RE, Dalmasso EA, Fu S, Pham T, Mei J, Ho JJ, Zhang W, Lopez P, Ho DD.** Contribution of human alpha-defensin 1, 2, and 3 to the anti-HIV-1 activity of CD8 antiviral factor. *Science* 298: 995–1000, 2002.

J Appl Physiol 102: 2361–2368, 2007.
First published March 1, 2007; doi:10.1152/japplphysiol.00615.2006.

Adrenomedullin insufficiency increases allergen-induced airway hyperresponsiveness in mice

Hiroshi Yamamoto,[1] Takahide Nagase,[2] Takayuki Shindo,[3] Shinji Teramoto,[1] Tomoko Aoki-Nagase,[1] Yasuhiro Yamaguchi,[1] Yoko Hanaoka,[1] Hiroki Kurihara,[4] and Yasuyoshi Ouchi[1]

Departments of [1]Geriatric Medicine, [2]Respiratory Medicine, and [4]Physiological Chemistry and Metabolism, Graduate School of Medicine, University of Tokyo, Tokyo; and [3]Department of Organ Regeneration, Shinshu University Graduate School of Medicine, Nagano, Japan

Submitted 2 June 2006; accepted in final form 25 February 2007

Yamamoto H, Nagase T, Shindo T, Teramoto S, Aoki-Nagase T, Yamaguchi Y, Hanaoka Y, Kurihara H, Ouchi Y. Adrenomedullin insufficiency increases allergen-induced airway hyperresponsiveness in mice. *J Appl Physiol* 102: 2361–2368, 2007. First published March 1, 2007; doi:10.1152/japplphysiol.00615.2006.—Adrenomedullin (ADM), a newly identified vasodilating peptide, is reported to be expressed in lungs and have a bronchodilating effect. We hypothesized whether ADM could be involved in the pathogenesis of bronchial asthma. We examined the role of ADM in airway responsiveness using heterozygous ADM-deficient mice ($AM^{+/-}$) and their littermate control ($AM^{+/+}$). Here, we show that airway responsiveness is enhanced in ADM mutant mice after sensitization and challenge with ovalbumin (OVA). The immunoreactive ADM level in the lung tissue after methacholine challenge was significantly greater in the wild-type mice than that in the mutant. However, the impairment of ADM gene function did not affect immunoglobulins (OVA-specific IgE and IgG1), T helper 1 and 2 cytokines, and leukotrenes. Thus the conventional mechanism of allergen-induced airway responsiveness is not relevant to this model. Furthermore, morphometric analysis revealed that eosinophilia and airway hypersecretion were similarly found in both the OVA-treated ADM mutant mice and the OVA-treated wild-type mice. On the other hand, the area of the airway smooth muscle layer of the OVA-treated mutant mice was significantly greater than that of the OVA-treated wild-type mice. These results suggest that ADM gene disruption may be associated with airway smooth muscle hyperplasia as well as enhanced airway hyperresponsiveness. ADM mutant mice might provide novel insights to study the pathophysiological role of ADM in vivo.

asthma; airway hyperresponsiveness; remodeling; adrenomedullin; knockout mouse

ADRENOMEDULLIN (ADM) is a newly identified vasodilating peptide initially isolated from the extracts of human pheochromocytoma tissue (14). This peptide, which consists of 52 amino acids in human, belongs to the CGRP/CT superfamily of peptides including calcitonin (CT), amylin, and CT gene-related peptide (CGRP). ADM mRNA is demonstrated in a number of tissues, abundant in adrenal medulla, atrium, and lung (7), whereas ADM also circulates in the plasma (13). McLatchie et al. demonstrated that the CT-receptor-like receptor functions as an ADM receptor in the presence of receptor-activity-modifying protein 2 (17). They also demonstrated that the expression of receptor-activity-modifying protein 2 component was strongly recognized in the lung. Although it is speculated that ADM plays an important role in the lung tissue, the exact roles of ADM gene function on airway inflammation and airway remodeling remain little known.

In animals, Kanazawa and colleagues have reported that ADM inhibits histamine- or acetylcholine-induced bronchoconstriction in anesthetized guinea pigs (12) and that its bronchodilating effect is as potent as isoproterenol. They also demonstrated that the precursor of ADM, i.e., proadrenomedullin NH_2-terminal 20 peptide, has the same properties to induce bronchodilation (11). Furthermore, it has been demonstrated that ADM has the inhibitory effect on antigen-induced microvascular leakage and bronchoconstriction in guinea pigs (20). In humans, it was also reported that human plasma ADM levels correlated negatively with the degree of airway obstruction, as indicated by forced expiratory volume in 1 s; the plasma ADM concentration was associated with the severity of human asthma. This suggests that the level of ADM excretion may affect the degree of asthma severity or that asthma-related bronchoconstriction and/or hypoxia increases the ADM levels as a compensative mechanism (3). Thus it is reasonably assumed that ADM, proadrenomedullin NH_2-terminal 20 peptide, or their derivatives could be the new-generation bronchodilators used in the clinical settings. Meanwhile, the biological roles of innate ADM peptides based on ADM gene function in vivo remain unclear.

Because the familial or the genetic background is potentially associated with the etiology of asthma, a number of genes have been explored for the association of asthma (4). However, the exact molecular mechanisms underlying bronchial asthma still remain to be elucidated. We therefore hypothesized whether ADM gene could be involved in the pathogenesis of asthma.

Since the airway hyperresponsiveness (AHR) and inflammation including eosinophil infiltration are major characteristics of asthma (5, 6, 16), we examined the role of ADM in airway responsiveness using murine model of asthma. Although we recognized that homozygous ADM-deficient mice ($AM^{-/-}$) are best suitable for the current experiments, they are unfortunately embryonic lethal (23). We therefore performed the following experiments using heterozygous ADM-deficient mice ($AM^{+/-}$) and their littermate wild-type control ($AM^{+/+}$).

Then, we examined the relationship between the AHR and the lung inflammation including eosinophil infiltration and other inflammatory mediators in mutant mice and control mice. In murine lung model of allergen-induced hyperresponsive-

Address for reprint requests and other correspondence: H. Yamamoto, Dept. of Geriatric Medicine, Graduate School of Medicine, Univ. of Tokyo, 7-3-1 Hongo, Bunkyo-ku, Tokyo, Japan 113-8655 (e-mail: hyamamot-tky@umin.ac.jp).

The costs of publication of this article were defrayed in part by the payment of page charges. The article must therefore be hereby marked "*advertisement*" in accordance with 18 U.S.C. Section 1734 solely to indicate this fact.

ness, OVA challenge induces an eosinophilic inflammation, bronchial hyperresponsiveness, and production of specific IgE (15). However, the precise role of various types of inflammatory cells and mediators involved in the pathophysiology of AHR remains to be fully determined. Thus we further examined the other inflammatory mediators including immunoglobulins (OVA-specific IgE and IgG1), T helper (Th) 1 and Th2 cytokines, and leukotrienes (LTs).

In addition, the association of morphological changes with AHR in the murine model was examined. Because ADM is known to have anti-proliferative effect on smooth muscle cells and fibroblasts, altered ADM function may affect cell kinetics on airway wall, which may contribute to induction of AHR in the mice.

MATERIALS AND METHODS

Animals. Heterozygous ADM-deficient mice ($AM^{+/-}$) were established as previously described (23). Briefly, a targeting vector was constructed to replace the 2.4-kb fragment encompassing the 1.3-kb 5′-flanking region, exons 1–3, and part of exon 4 of proadrenomedullin with the neomycin resistance gene. The plasmid was linearized and then introduced into 129/Sv-derived SM-1 embryonic stem cells by electroporation. Homologous recombinants were identified by Southern blot analysis, and two independently targeted clones were injected into C57/BL6 blastocysts to generate chimeric mice. Male Chimeras were crossbred with C57/BL6 females, and germ-line transmission was verified by Southern blot analysis. All experiments were approved by the University of Tokyo Ethics Committee for Animal Experiments. For genotyping, genomic DNAs were isolated from biopsied tail and subjected to PCR amplification. The animals were maintained on a light-dark cycle with light from 0700 to 2000 at 23°C. Mice were fed with a standard laboratory diet and water ad libitum. Mutant mice and their littermate controls ($AM^{+/+}$), between 4 and 12 wk of age, were used in the current study. There was no difference in the body weight between the wild-type group and the mutant one [$AM^{+/+}$ saline (n = 11), 30.18 ± 0.76 g; $AM^{+/-}$ saline (n = 11), 30.36 ± 0.82 g; $AM^{+/+}$ OVA (n = 14), 29.00 ± 1.28 g; $AM^{+/-}$ OVA (n = 14), 29.79 ± 0.79 g].

Sensitization and antigen challenge. To develop allergen-induced asthma model mice, we performed allergen sensitization and inhalational antigen challenge as previously described (2). Briefly, on *day 1*, $AM^{+/+}$ or $AM^{+/-}$ mice were randomly selected and sensitized with intraperitoneal (ip) injection of 0.5 ml solution containing 0.1 mg OVA mixed with aluminum hydroxide (2 mg/ml). On *day 8*, the mice were subsequently boosted with the same mixture. On *days 13* and *14*, these sensitized mice were placed in an 18 × 11 × 11 cm plastic chamber and were challenged for 60 min with aerosolized 1% OVA dissolved in saline, generated with an ultrasonic nebulizer (NE-U17, Omron). Others received ip injection of saline and saline aerosols in the same manner. On *day 15*, we performed measurement of bronchial responsiveness or bronchoalveolar lavage (BAL).

Animal preparation. Animals were anesthetized with pentobarbital sodium (25 mg/kg ip) and ketamine hydrochloride (25 mg/kg ip) in combination and then paralyzed with pancuronium bromide (0.3 mg/kg ip). After tracheostomy, an endotracheal metal tube (inside diameter of 1 mm, length of 8 mm) was inserted in the trachea. Animals were mechanically ventilated (model 683, Harvard Apparatus, South Natick, MA) with tidal volumes of 10 ml/kg and frequencies of 2.5 Hz. An incision was made on the abdominal wall, then the diaphragm of the bilateral chest was incised and the chest was widely opened. Positive end-expiratory pressure of 2 cmH_2O was applied by placing the expired line underwater. During the experiments, oxygen gas was continuously supplied to the ventilatory system. A heating pad was used to maintain the body temperature of animals. Tracheal pressure was measured with a piezoresistive micro transducer (Endevco 8510B-2, San Juan Capistrano) placed in the lateral port of the tracheal cannula. Tracheal flow was measured by means of a Fleisch pneumotachograph (model no. 00000, Metabo SA, Lausanne, Switzerland). All signals were amplified, filtered at a cutoff frequency of 100 Hz, and converted from analog to digital with a converter (DT2801-A, Data Translation, Marlborough, MA). The signals were sampled at a rate of 200 Hz and stored on an IBM-AT compatible computer. Lung resistance (R_L) and elastance were measured as previously described (19).

Airway responsiveness to methacholine administration. At the start of the protocol, two deep inhalations (3 times tidal volume) were delivered to standardize volume history. All animals were then challenged with saline aerosol for 2 min. Aerosols were generated by an ultrasonic nebulizer (Ultra-Neb100, DeVilbiss, Somerset, PA) and delivered through the inspiratory line into the trachea. Measurements of 10-s duration were sampled during tidal ventilation 1 min after administration of saline aerosol. This represented the baseline measurement. Then, each dose of methacholine (MCh) aerosol was administered for 2 min, and measurements were performed 1 min after each MCh inhalation in a dose-response manner (0.3125, 0.625, 1.25, 2.5, 5, 10, 20, 40, and 80 mg/ml). Airway responsiveness was assessed using the concentration of MCh required to increase R_L to 200% of baseline values ($EC_{200}R_L$) (18).

BAL fluid. BAL was performed using 1 ml of PBS 5 times in each group. In each animal, ~90% (4.5 ml) of the total injected volume was consistently recovered. After BAL fluid (BALF) was centrifuged at 450 *g* for 10 min, the total and differential cell counts of the BALF were determined from the cell fraction. The supernatant was stored at −80°C until assays were performed. The concentration of protein was measured by Bradford's method using bovine serum albumin as a standard.

Assay of total immunoglobulin E (IgE) in BALF. Total amount of IgE was assayed followed by the PharMingen protocol (http://www.bdbiosciences.com/pharmingen/protocols/Mouse_IgE_ELISA.shtml). The purified anti-mouse IgE capture monoclonal antibody (BD PharMingen, catalog no. 02111D, clone R35-72) was used for the assay. The antibody titers were calculated by comparison with standard samples using serum of an OVA-immunized mouse and analyzed with the Microplate Manager software for the Macintosh computer (Bio-Rad). The detection limit of the ELISA assays for IgE was 4.59 ng/ml.

Assay of OVA-specific IgE in serum. OVA-specific IgE was assayed in a manner similar to the PharMingen protocol of IgE. Briefly, 96-well flat-bottomed ELISA plates were coated with the purified anti-mouse IgE capture monoclonal antibody (BD PharMingen, catalog no. 553413, clone R35-72) and conjugated with biotinylated OVA and SAv-HRP. We measured the absorbance on the microplate

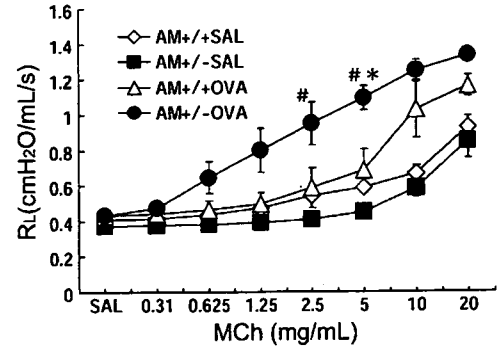

Fig. 1. Methacholine (MCh) dose response curves for lung resistance (R_L) in the wild-type and the heterozygous adrenomedullin (ADM) mutant mice. SAL, saline; OVA, ovalbumin. *$P < 0.05$ compared with the R_L in the same MCh dosage of $AM^{+/+}$ OVA group. #$P < 0.05$ compared with the R_L in the same MCh dosage of $AM^{+/-}$ SAL group.

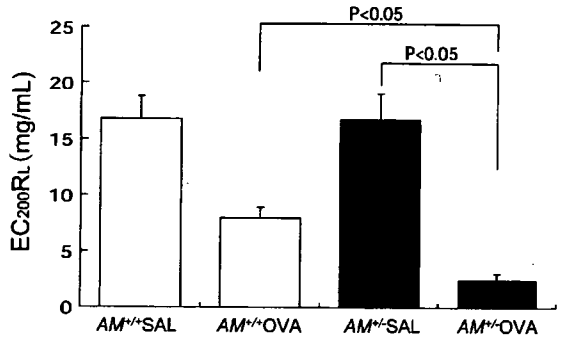

Fig. 2. $EC_{200}RL$, Concentration of MCh required to increase RL to 200% of baseline values. *$P < 0.05$ compared with the value of $AM^{+/+}$ OVA group. #$P < 0.05$ compared with the value of $AM^{+/-}$ SAL group.

reader set at 450 nm. The detection limit of the ELISA assays for OVA-specific IgE was 20 U/ml.

Assay of OVA-specific IgG1 in serum. An enhanced protein-binding ELISA plate was coated with the purified OVA. The plate was then blocked with 200 μl of blocking buffer per well. Samples or standards were put in each well at various dilutions in blocking buffer. Horseradish peroxidase-conjugated anti-mouse IgG1 (BD PharMingen, catalog no. 559626, clone X56) was diluted to 2 μg/ml in blocking buffer and was added respectively. The plate was incubated at room temperature for 30 min. Substrate buffer was added to develop color reaction at room temperature for 20–30 min. We measured the absorbance on the microplate reader set at 450 nm. The antibody titers were calculated by comparison with standard samples using serum of an OVA-immunized mouse and analyzed with the Microplate Manager software for the Macintosh computer (Bio-Rad). The detection limit of the ELISA assays for IgG1 was 142 U/ml.

Assays of LTs, IL-4, -5, and -13, and IFN-γ in BALF. LTC4/D4/E4 was measured using enzyme immunoassay kit (GE Healthcare Bio-Sciences, catalog no. RPN 224). Detection limit of LTC4/D4/E4 was 10 pg/ml. IL-4 and -5 and IFN-γ in BALF were measured using ELISA kits [Pierce Biotechnology, catalog no. EMIL42 (IL-4), EMIL52 (IL-5), EM1001 (IFN-γ)]. IL-13 in BALF was measured using mouse IL-13 immunoassay kit (Genzyme TECHNE, catalog no. 10003). Detection limits of the ELISA assays for IL-4, IL-5, IL-13, and IFN-γ were 15, 20, 7.8, and 37 pg/ml, respectively.

Assay of tissue ADM. Using lung specimens before and after MCh challenge, immunoreactive ADM (ir-ADM) levels in the lung tissues were measured using ADM[1–50](Mouse) RIA kit (Phoenix Pharmaceuticals, catalog no. RK-010-31). Before the assay, tissue sections were soaked in the 1.0 ml of 0.1 M acetic acid solution and were bathed in the 100°C water bath for 10 min. Then they were cooled down with ice, homogenized, and centrifuged at 13,000 *g* for 5 min at 4°C. The supernatant was used for the assay. The values of the ir-ADM were expressed as the quantity per gram wet tissue samples.

Semi-quantitative assessment of eosinophilia and airway mucus hypersecretion. Whole samples of tissue were fixed in 10% phosphate-buffered formalin (pH 7.4), embedded in paraffin, and cut into 4-μm sections. The sections were stained with hematoxylin and eosin, Luna, or periodic acid Schiff (PAS) and Alcian Blue co-staining. Each slide was provided for the count of cells. Eosinophil infiltration of the peribronchial tissue was estimated by using Luna stained slides. Goblet cell hyperplasia and airway mucus hypersecretion were assessed by inspecting PAS and Alcian blue stained slides. All slides were observed by the two uncensored persons and assessed by their subjective scoring from 0 (none) to 3 (abundant) under the microscope (Nikon). In terms of the reproducibility of this assessment, inter- or intraobserver variances were <5%.

Morphometric analysis of airway walls. Each section was also stained with Masson's trichrome for morphometric analysis and observed by systemic manner. The whole slide was scanned thoroughly and membranous bronchioles were carefully selected for the analysis. All selected regions are digitally photographed by the Nikon microscope. Measurements were performed by Image J software (version 1.37v, National Institutes of Health), using an IBM-compatible computer equipped with a digitizing tablet. Measurements are as follows: *1*) Abm means the area surrounded by the airway basement membrane, whose perimeter is Pbm; *2*) Amo means the area surrounded by the airway smooth muscle outline, whose perimeter is Psm; *3*) Ai means the internal airway lumen area, whose perimeter is Pi; *4*) the area of epithelial cells (Ae) is calculated by Abm − Ai, the area of smooth muscles (Asm) is also calculated by Amo − Abm; *5*) airway longer diameter is DL, shorter one is Ds. Airway size was standardized by comparing Abm, i.e., Ai/Abm or Ae/Abm or Asm/Abm. Seventy-eight of 144 selected airway sections appeared in the slides were excluded by the following criteria: the short-to-long luminal diameter ratio (Ds/DL) was under 0.6 or the borders ill-defined. When we deal with the smooth muscle bundles, we carefully outlined the edge of the smooth muscle layer, and if we encountered the interruption of the locus, we followed it smoothly to the basement membrane to maximally exclude extracellular matrix. If the interruption was longer than 10% of Pbm, we discarded the sections like this. All the other components were applied for the analysis. In the same way, analysis was performed for immunohistochemically stained sections.

We assessed the number of cells in the airway smooth muscle layer by counting the number of nuclei in the layer. To standardize by airway size, the nuclear cell count (NCC) was divided by Pbm^2; i.e., NCC/Pbm^2. The standardized number of nuclear cells in the airway smooth muscle layer was compared among four groups, i.e., saline-treated wild-type, saline-treated ADM mutant, OVA-treated wild-type, OVA-treated ADM mutant mice.

Immunohistochemical staining for alpha-smooth muscle actin. Immunohistochemistry was performed using monoclonal antibodies against alpha-smooth muscle actin (α-SM actin) (DAKO Cytomation, code M0851, clone 1A4). After tissue sections were deparafinized and rehydrated, antigen retrieval was accomplished by 15-min incubation at 121°C in 0.01 M citrate buffered solution (pH 6.0). Endogenous peroxidase activity was blocked by incubation in methanol containing 3% H_2O_2. Anti-α-SM actin antibody of 1:50 dilution was prepared together with ENVISION+/horseradish peroxidase kit for Mouse (DAKO Cytomation, catalog no. K4000), then incubated with normal mouse serum for 60 min. This conjugate was added on each section and visualized by DAB. Labeling controls were performed under the

Table 1. *Total cell counts and cell fractions in BALF in each experimental group*

	TCC (×10⁴)	Mφ, %	Lym, %	Eos, %	PMN, %
$AM^{+/+}$ saline (n = 5)	4.94±1.91	96.02±2.82	4.32±2.67	0.02±0.00	0.26±0.21
$AM^{+/-}$ saline (n = 5)	4.82±0.54	91.96±2.51	7.24±2.25	0.10±0.00	0.82±0.48
$AM^{+/+}$ OVA (n = 5)	40.20±18.22†	70.58±15.00	2.84±1.87	25.88±14.88*	0.72±0.45
$AM^{+/-}$ OVA (n = 6)	21.13±8.75	60.02±12.41†	4.00±1.60	35.30±12.84†	0.70±0.28

Values are means ± SE. TCC, total cell count; Mφ, macrophages; Lym, lymphocytes; Eos, eosinophils; PMN, polymorphonuclear cells; BALF, broncho alveolor lavage fluid. †$P < 0.05$ compared with the saline group in the same strain of animals. *$P < 0.01$ compared with the saline group in the same strain of animals.